THESIS

FATIGUE RELIABILITY AND POST-FRACTURE RESIDUAL CAPACITY OF A TWO-GIRDER STEEL BRIDGE

Submitted by

Lena F. Hartung

Department of Civil and Environmental Engineering

In partial fulfillment of the requirements

For the Degree of Master of Science

Colorado State University

Fort Collins, Colorado

Fall 2016

Master's Committee:

Advisor: Hussam Mahmoud

Rebecca Atadero
Kelly Strong

ABSTRACT

FATIGUE RELIABILITY AND POST-FRACTURE RESIDUAL CAPACITY OF A TWO-GIRDER STEEL BRIDGE

Due to the immense and always increasing traffic volume, bridges are permanently subjected to repetitive loadings. These high numbers of cyclic loads can cause initiation of fatigue cracks. If these flaws remain undetected they may become through-thickness cracks and further propagate, if left unrepaired, until they eventually arrest when entering a high compression zone or further propagate to fracture of the entire member. The criticality of a full member fracture is not well defined nor agreed upon. Previous failure cases have demonstrated the ability of two-girder steel bridges to withstand full girder fracture of one of the two girders without structural collapse. Other cases, however, have shown the criticality of a complete girder failure on complete system collapse. Due to uncertainties in bridge redundancy and the ability to develop alternative load path, the American Association of State Highway and Transportation Officials (AASHTO) attempts to prevent fracture or collapse by classifying bridges with respect to their redundancy into fracture critical bridges (FCB) and decreasing their inspection periods. However, this leads to higher construction and maintenance costs for the owners of FCBs. The level of uncertainty in bridge performance when one of its two girders suffer complete fracture should be represented in a probabilistic manner to evaluate the probability of fatigue crack growth and the potential for system collapse. To that end, in this thesis probabilistic analysis is used to assess the crack propagation behavior in a girder of a two-girder steel bridge by conducting finite element Monte Carlo simulations. The simulations account for the scatter in the load and the resistance by treating

those uncertainties as random variables with predefined statistical distributions. The results of the analysis are presented in terms of probability of failure versus inspection intervals for various levels of material fracture toughness. The results provide an illustration on the use of the proposed methodology to devise inspection intervals based on desired probability of failures. Additionally, the post-fracture redundancy is evaluated by comparing the resulting equivalent plastic strain to the failure strain of steel. The results show that the bridge provides sufficient redundancy to redistribute the load after full depth fracture of a FC member.

ACKNOWLEDGEMENTS

I would like to thank my advisor Dr. Hussam Mahmoud for his continuous and valuable support throughout the work on this thesis. I would also like to thank my committee members Dr. Rebecca Atadero and Dr. Kelly Strong for their effort and the time they spent on reviewing my work. Furthermore, I want to thank my classmates and friends Dr. Mehrdad Memari, Hassan Masoomi and Akshat Chulahwat who helped me with coding and the finite element analysis. Finally, I want to thank my family and my closest friends for their continuous support. Without their support I would not be where I am today.

TABLE OF CONTENTS

LIST OF TABLES

LIST OF FIGURES

INTRODUCTION

1.1 Motivation

In the first half of the 20th century several bridge failures caused a nationwide concern over vulnerability of steel bridges. One famous example is the collapse of the Point Pleasant Bridge over the Ohio River in 1967. The collapse was one of the deadliest accidents in the history of bridge failures with the death of 46 persons. Examinations of the failure have shown that the brittle fracture of a single eyebar, which was part of the supporting system of the main span, caused the whole structure to collapse (NTSB, 1967). The reason for the complete failure was attributed to the lack of redundancy in the bridge. As a consequence of the Point Pleasant Bridge collapse and other bridge failures, the American Association of State Highway and Transportation Officials, AASHTO, started to classify bridges more strictly so that bridges vulnerable to complete collapse can be identified. A new category for fracture critical bridges (FCB) was introduced. A FCB is defined as a bridge with at least one fracture critical member (FCM). Whereas a FCM is defined as a "component in tension whose failure is expected to result in the collapse of the bridge or the inability of the bridge to perform its function" (AASHTO, 2012). This implicated that from this point on, two-girder steel bridges were classified as nonredundant and fracture critical (FC).

In reference to the National Cooperative Highway Research Program (NCHRP) Synthesis 354, about 11% of all steel bridges in the United States are classified as FC and 83% of those bridges are two girder bridges (Connor, Dexter, & Mahmoud, 2005). Following the National Bridge Inspection Standards (NBIS) 2012, FCBs require biannual hands on field inspections. The term hands on implies the inspection with the human eye, where the distance between the inspected object and the human eye is not larger than one human arm length. Since the inspection has to be

conducted by highly qualified professionals, the inspections are highly cost intensive and is usually two to five times higher for bridges with FCMs than for bridges without FCMs (Connor et al., 2005).

Even though AASHTO considers FCBs as nonredundant, there are several examples, which have shown that the fracture of one member does not always cause the whole structure to fail. Other structural components such as the deck, floor beams and stringers are often able to carry the sudden additional load (Connor, 2005).

It is obvious that the classification of bridges with respect to their redundancy is not simple. The justification for FCB is qualitative rather than based on a coherent quantitative strategy. The conservative approach in the past considered load path redundancy as the only form of redundancy when classifying bridges as fracture critical. However, research has shown that these bridges can still provide structural redundancy that can prevent collapse in the case that one of the main supporting members fails (Lwin, 2012). As a consequence of this, FCB are generally defined as nonredundant, although the inherent structural redundancy in them can be at an acceptable level. While classifying a bridge as fracture critical does lower the probability of complete collapse, this classification can lead to shorter bridge inspection intervals than actually necessary. A closer investigation resulting in a better understanding of the post-fracture redundancy of two-girder steel bridges could therefore save bridge owners and tax payers significant amount of money.

1.2 Objectives and Scope of Thesis

The overall objective of this study is to propose a methodology for determining inspection intervals for fracture critical bridges that is based on probabilistic fracture mechanics. This would allow departments of transportations and bridge owners to devise risk-informed inspection plans

to ultimately save substantial amount of funds and resources. The thesis can be subdivided into following scopes:

- Create a 3D numerical finite element model of a two-girder steel bridge.
- Implementing fatigue loading in the model in accordance with the design requirements specified in AASHTO.
- Conduct Monte Carlo simulations using Latin Hypercube Sampling in which the Young's modulus and the dynamic amplification factor are treated as random variables in the finite element model.
- Introduce a crack in the model, representing fatigue cracking, to compute the stress intensity factor at the crack tip for incremental crack growth.
- Utilize the Paris Law to determine the number of cycles versus crack length while treating the Paris law constants, C and m, as random variables.
- Estimate the critical crack length and the number of cycles to failure for various material toughness values.
- Compute the probability of failure and the corresponding reliability index for different inspection intervals.
- Evaluate the reserve capacity of the bridge as function crack length by comparing the equivalent plastic strain to the failure strain of the steel.

1.3 Organization of Thesis

The thesis is structured in 5 chapters. The first chapter presents the motivation for this work, defines the individual objectives and outlines the organization of the work. Chapter 2 consists of a literature review to provide a better understanding on the topics of fatigue and fracture and

reliability analysis. The chapter introduces the topic, a historical background, as well as an overview of previous studies. It also covers the fatigue requirements in the AASHTO LRFD Bridge Design Specification (AASHTO, 2012) and the theory of Linear Elastic Fracture Mechanics (LEFM) including the energy release rate and the stress intensity factor. The Paris' Law is explained to make a connection between the applied load and the remaining fatigue life. In addition, Chapter 2 provides an introduction to reliability analysis including the definition of failure, Monte Carlo simulation and Latin Hypercube Sampling. Chapter 3 describes the numerical 3D finite element model of the bridge. The section contains details about bridge geometry, loading, and assumptions and simplifications made realize the study. The model is outlined with the focus placed on the implementation of the crack and crack propagation in the model. Chapter 4 summarizes the probabilistic simulation methodology. It provides the individual steps necessary to proceed from the results of the Finite Element Analysis (FEA) to the probability of failure, the reliability index, and the redundancy assessment. The results of this thesis are presented in Chapter 5. Explanations and discussions of the findings are provided and supported by figures and tables for visualization purposes. Chapter 6 summarizes the main findings of this study and an overall conclusion is drawn.

BACKGROUND AND LITERATURE REVIEW

2.1 Introduction and historical background

Fatigue is the process of crack formation and crack propagation in materials subjected to cyclic loading. One of the most common structures in civil engineering exposed to repetitive loading are bridges (Fisher, Kulak, & Smith, 1998). Due to the immense traffic volume, bridges experience high numbers of repetitive loads. These high numbers of cycles can cause existing weld flaws to become through-thickness cracks and further propagate, leading to reduction of the uncracked cross-section of the member. Failure occurs when the reduced cross-section is no longer able to carry the internal forces and the crack propagates in an unstable manner (Fisher, 1998). Fatigue cracking can occur at stress ranges that are way below stresses related to failure under static loading conditions. The fatigue performance of steel structure is highly dependent on the presence of pre-existing cracks or crack-like discontinuities. A consequence of this is that only a small part of the total fatigue life is spent on crack initiation (Fisher et al., 1998).

The phenomenon of fatigue crack growth has already been observed more than 100 years ago. Wöhler (1870) conducted one of the first studies on the topic of fatigue in the late 19th century. In his study on a railway rolling stock, Wöhler found that high stress concentrations caused failure although the measured stresses were far below the yield strength of the material (Wöhler, 1870).

Before the 1950's, when welding was not yet a popular fabrication method, most steel bridges were designed using mechanical fasteners (FHWA, 2015). The change from mechanical fasteners to welding confronted engineers with new challenges since the welding process induces residual stresses and flaws into the steel and the structure's susceptibility to fatigue cracking increases. Thus, fatigue design specifications were developed to provide engineers with design

guidelines to avoid fatigue failure. The first fatigue design specifications in North America were based on examinations of welded steel details conducted in the 1930's and after World War II (Fisher et al., 1998). However, the specifications were based on a limited amount of test data and small specimens. In 1968 the fatigue test program sponsored by the National Cooperative Highway Research Program was established at Lehigh University (Fisher et al., 1998). This program allowed the examination of fatigue cracks and their behavior on a larger scale. The results showed that the design rules used until that point were incorrect for numerous bridge details and also gives an explanation as to why many bridges designed before 1975 failed in fatigue (Fisher et al., 1998).

One example of a brittle bridge collapse is the Mianus River Bridge on I-95 in Connecticut in 1983. Poor maintenance was responsible for a clogged drain, which resulted in packout corrosion in a pin and hanger assembly, which caused one of the plates to slip off the pin leading to the collapse. It is obvious that the pin and hanger assembly was a FCM since its failure caused a complete system collapse (Failla, 1985).

Another example is the collapse of the Point Pleasant Bridge over the Ohio River in 1967. The failure investigation has shown that the brittle fracture of a single eyebar, which was part of the supporting system of the main span, caused the whole structure to collapse (NTSB, 1967). Both catastrophes occurred because the bridges did not provide sufficient redundancy to redistribute the load after failure.

Despite the noted complete bridge collapse cases, there are several events where brittle fracture occurred but luckily did not result in a collapse of the whole structure. The US-52 bridge in St. Paul, Minnesota survived a full depth fracture without collapse (Connor et al., 2005). The bridge dropped 6.5 in but remained stable. Another example of a bridge failure that did not end in a collapse is the I-79 bridge in Pittsburg, Pennsylvania (Connor et al., 2005). The bridge also

experienced a full-depth fracture, yet there was no noticeable deformation. In those two cases, other structural components were able to support the additional load after the development of a full depth crack. Both bridges were two-girder steel bridges and classified as FCB. These examples show that the classification of bridges by only considering load path redundancy is not sufficient.

Following the Point Pleasant Bridge failure in 1967, much research was conducted regarding post-fracture redundancy, fracture toughness of steel, bridge inspection and maintenance. It was well known that material properties are an important aspect in brittle fracture and therefore there was great interest in increasing the understanding of fracture toughness of steel. The U.S. Department of Transportation FHWA sponsored a study at Lehigh University with the goal to establish a common measurement for the fracture toughness along with a measuring method and to assess the fracture toughness of commonly used bridge steel (Robert, Irwin, Krishna, & Yen, 1974). One of the results of this research was a database with fracture toughness values for several steel types.

Another research on fracture toughness of steel was conducted by Barsom (1975). The study showed that fracture toughness of bridge steel is affected by temperature and strain range. The results were used to propose an equation to compute the critical fracture toughness of bridge steel using measured Charpy V-notch values. A reasonable minimum fracture toughness requirements were suggested, which were adopted by FHWA and AASHTO. The introduction of minimum Charpy V-notch (CVN) toughness requirements for welds and base metals was supposed to ensure sufficient resistance to fracture since materials with higher fracture toughness can tolerate longer cracks without failing. The CVN requirements in today's specifications for non FCM are basically the same as the original ones form 1974 (Connor et al., 2005).

A further result of the Point Pleasant Bridge failure was the establishment of the National Bridge Inspection Standards (NBIS) through the FHWA, which came into effect in 1971. The NBIS document specifies the procedures and the frequency for inspections, minimum qualifications for the bridge inspectors and new reporting and documentation requirements.

Another regulation to increase safety that was developed as a consequence of severe bridge failures, is the fracture control plan (FCP). Research has shown that fracture toughness is only one component out of many that may cause brittle fracture. The need for a specification that covers all aspects of brittle fracture was recognized and the FCP was introduced in the 1970's. The document regulates design, fabrication, materials, inspection, and service conditions. Case studies showed that if this FCP would have been in operation earlier several bridge failures would not have occurred (Rolfe & Barsom, 1999).

All the above listed requirements are necessary to ensure safety in the design and maintenance of FCBs. However, those regulations led to a significant cost increase for bridge owners. Therefore, it is essential that those regulations are only applied if necessary. Currently, the AASHTO bridge design specification determines which of the above regulations have to be met, depending on the redundancy of the bridge. Because of this, much research has been published with the focus on post-fracture redundancy of FCBs. A detailed annotated literature review is provided by Connor et al. (2005). The researchers were interested in the load redistribution and the potential for collapse. Hartley and Ressler (1989) reviewed numerous articles with this topic and concluded that no coinciding definition of redundancy existed because redundancy is a measurement that is not easy to quantify.

Cha et al. (2014) published a paper discussing the postfracture redundancy of a simple span truss bridge. This study assessed the redundancy of a full-scale bridge by conducting controlled

fracture tests. Furthermore, a numerical model of the bridge was used to determine the postfracture behavior. The results showed that the structure had significant internal and load path redundancy although it was categorized as a fracture critical bridge (FCB). It was suggested to reconsider the categorization of FCB or at least the required inspection interval.

Daniels et al. (1989) proposed design instructions and suggested rating criteria for redundant bracing systems for two-girder steel bridges. They conducted research on the post-fracture redundancy of single span steel two-girder highway bridges. An analytical model with a close to full-depth fracture on one of the girders was used to conduct the study. The results proved that bracing can provide sufficient redundancy if designed accurately. It was concluded that a new rating system for redundancy is needed.

Besterfield et al. (1991) applied probabilistic finite element method to examine the fatigue crack growth reliability of an unstiffened plate with a through thickness single edge crack. In their study the initial and final crack lengths, initial crack angle and position, material properties, crack growth law, crack direction law and loading are treated as random variables. The output of this study was the probability of fatigue failure of the plate.

More research on fatigue reliability was conducted by Feng, Garbatov, & Guedes Soares (2012). In their study the finite element method is used to define the correlation between multiple cracks by calculating the stress intensity factors. The statistical evaluation of the crack propagation rate was done by Monte Carlo simulation. Subsequently, First Order Reliability Method (FORM) was utilized to compute the probability of failure. The analysis also accounted for residual stresses. The study examines parameters related to manufacturing, inspections, inspection interval, load level and target reliability acceptance.

Another study conducted by Mahmoud and Riveros (2014) examines the fatigue reliability of a single stiffened ship hull panel. The study focuses on investigating the crack propagation rate while accounting for the large scatter in loading, residual stresses, and material resistance. Finite element Monte Carlo simulation was used to conduct probability analysis in which the load and material properties are treated as random variables. Finally, Mahmoud and Riveros (2014) computed the probability of failure for a specific inspection interval. The result can be used to choose an inspection interval for a desired reliability index. The presented analysis framework in this thesis draws from the work conducted by Mahmoud and Riveros but for complete 3D two-girder steel bridges.

The literature review has shown that much research has been conducted on the post-fracture behavior of FCBs. The structural reliability was determined using experimental, numerical and analytical tools or combinations of such. The research conducted on bridges agrees on the fact that bridges, which are originally classified as non-redundant fracture critical, may still have sufficient level of redundancy to prevent complete system collapse when one girder is fully fractured. None of the researchers was able to propose a quantifying measurement of redundancy that became widely accepted but instead agreed that new, common definition of redundancy is needed. Research has also been conducted on crack propagation rate of stiffened and unstiffened panels. Probabilistic analysis was used to determine the fatigue reliability of the studied steel panels. The study by Mahmoud and Riveros (2014) provided precise tool to make decisions about increasing the inspection interval for structures susceptible to fatigue, whereby the maintenance costs can be decreased.

The research presented in this work not only provides new insight on post-fracture behavior of two-girder steel bridges but also provides results that can be used to develop a new bridge

inspection plan. In this study, numerical simulation and probabilistic analysis are used together. This enables to investigate the crack propagation while considering variation in the material properties and the load. The probability analysis is conducted using Monte Carlo simulation in which the load and the material properties are described by statistical distributions. Various results will be presented including contours of global deformations and stress concentrations, values of stress intensity factors as function of crack length, and plots of the probability of failure with respect to the inspection interval. The following sections provide the theoretical background needed to accomplish the study.

2.2 S-N Curves and Fatigue Categories

Early fatigue tests were conducted in the 19th century by Wöhler (1870) and as a result S-N curves were traditionally referred to as Wöhler curves. S-N curves are straight-line plots of stress range versus number of cycles to failure, represented on a log-log scale, for various bridge details. Failure as it pertains to S-N curves is defined by the development of a through-thickness crack. A typical S-N curve is plotted using data collected through applying cyclic loading in the laboratory to the detail in question. The test is repeated for a large number of stress ranges so that the all the failure points display as a line on the log-log scale. Typically, the first specimen is tested at a very high stress for which failure occurs at a low number of cycles. The stress range is then slowly decreased for every further specimen until one or two the specimens do not fail. The stress at which the specimen does not fail is called the fatigue threshold.

The relationship between the number of cycles and the stress range used in the AASHTO LRFD design specification for load induced fatigue is described by

$$N = \frac{n}{\mathbf{I}^{\mathbf{I}}} \qquad (2.1)$$

Where N is the number of cycles, A is the detail category constant and S is the difference between the maximum and the minimum applied stress. The values for the detail category constant are shown in Table 1 for units in MPa.

Researchers have studied the fatigue behavior of common bolted and welded connections typically used in bridges. In a bolted connection, the presence of a hole can be viewed as an initial flaw, from which crack initiation in the base metal could start. In welded connections, discontinuities resulting from the welding process can be the source of crack initiation. The AASHTO design specification classifies the details in eight fatigue categories: A, B, B', C, C', D, E and E', of which category A is the least susceptible to fatigue and category E' the most. The fatigue life curves for each detail category are shown in Figure 1. The horizontal lines in the plot mark the constant amplitude fatigue limit (CAFL), which is a threshold value below which fatigue damage would not be expected (i.e. infinite fatigue life).

It is important to mention that when one uses the S-N curves to determine the fatigue life the stress range that needs to be used results from the applied loads only since the stress concentration for the detail are already considered in the category.

Table 1 Detail category constants after (AASHTO, 2012)

Detail Category	Constant, A $(MPa)^3$	Threshold Stress (MPa)
A	$82.0x10^{11}$	165
B	$39.3x10^{11}$	110
B’	$20.0x10^{11}$	82.7
C	$14.4x10^{11}$	69.0
C’	$14.4x10^{11}$	82.7
D	$7.21x10^{11}$	48.3
E	$3.61x10^{11}$	31.0
E’	$1.28x10^{11}$	17.9

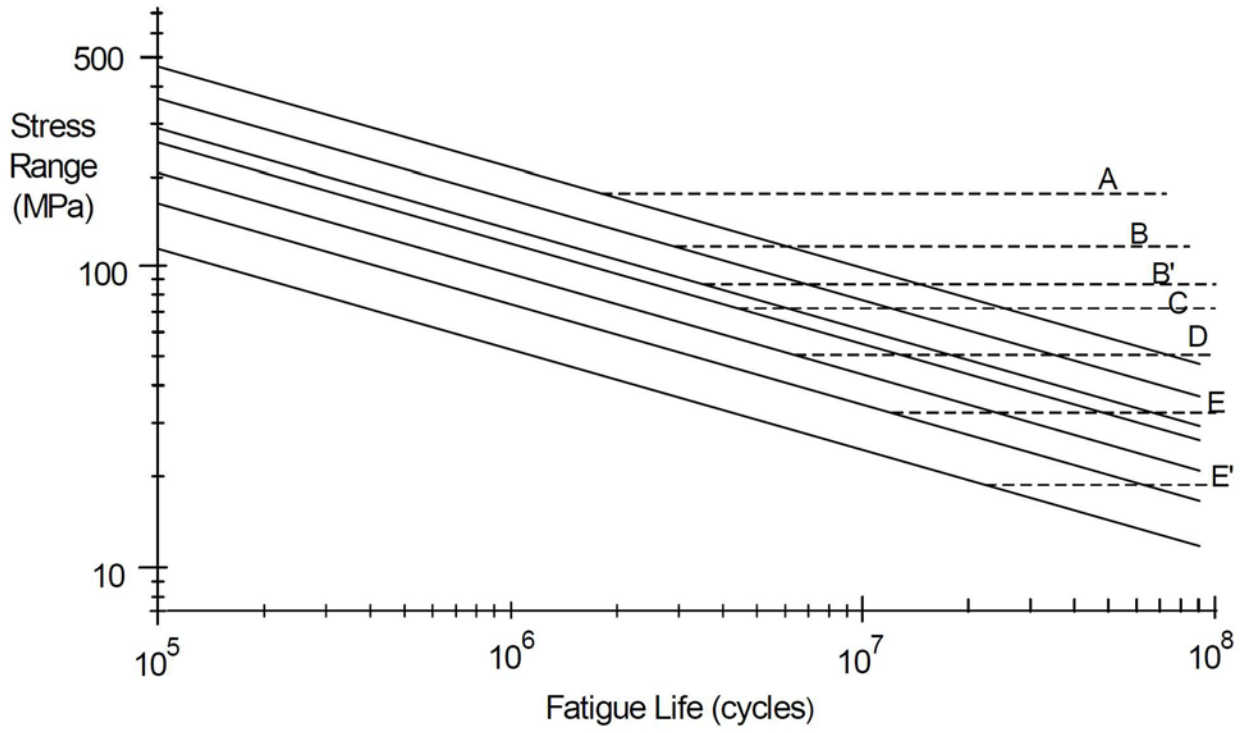

Figure 1 Fatigue life for the eight detail categories defined in AASHTO (Fisher et al., 1998)

Much research has been done on the fatigue life of different details and it is well agreed upon that the live load stress range is the controlling stress parameter when determining the fatigue life rather than the maximum absolute applied stress. Furthermore, the grade of steel does not have a significant influence on fatigue life.

2.3 Linear Elastic Fracture Mechanics

The theory of linear elastic fracture mechanics (LEFM) is a fracture analysis method applicable to materials following the Hooke's law, which means the overall structural behavior is linear elastic. LEFM is used to examine the behavior of the crack tip. The two most common approaches used to describe fracture in a linear elastic material are the energy approach developed by Griffith (1920) and the stress intensity approach proposed by Irwin (1956) (Anderson, 2005). The theory of LEFM studies the displacement, stress and strain at the tip of a crack in a linear elastic body as well as the rate of change in potential energy with the crack area. LEFM is applied where there is only minimal plastic deformation in the area around the crack tip. The theory of LEFM is always an approximation since even the most brittle materials experience some plastic deformation at the crack tip. However, the method is often used for nonlinear materials for which the plastic zone is considered negligible.

On an atomic level, fracture occurs when the applied stresses are sufficient enough to break the atomic bond. The cohesive strength σ_c of a material can be defined as (Anderson, 2005):

$$= \frac{\text{II}}{} \qquad (2.2)$$

Where E is the Young's modulus, λ is the distance between two atoms and x_o is the atom spacing at equilibrium. If λ is assumed to be approximately equal to x_o equation (2.2) can be simplified to

$$\approx \frac{\mathbf{I}}{\mathbf{I}} \qquad (2.3)$$

Equation (2.3) defines the cohesive strength for perfect materials without flaws. However, perfect materials do not exist and the actual fracture strength for brittle material is typically three to four times below the value resulting from equation (2.3) (Anderson, 2005). Flaws in the material cause stress concentrations, which amplify the stress locally and thereby decrease the material strength. The cohesive strength that needs to be overcome for fracture can be estimated as follows

$$= \frac{\overline{\mathbf{I}}}{\mathbf{I}} \qquad (2.4)$$

Where Υ_s is the surface energy per unit area

$$\mathbf{I}_n = \frac{\mathbf{I}}{\mathbf{I}} \mathbf{I}_1^{\mathbf{I}} \quad \sin \mathbf{I} \frac{}{\mathbf{I}} 1 \quad = \quad \frac{\mathbf{I}}{\mathbf{I}} \qquad (2.5)$$

The energy at which the material fractures is twice the surface energy since during fracture two surfaces are created.

2.4 Stress Concentration at the Crack Tip

Inglis (1913) was the first who conducted research on the effect of local stress concentration. For that purpose, he studied the stress field at the crack tip of an elliptical flaw in a flat plate. The geometry is shown in Figure 2.

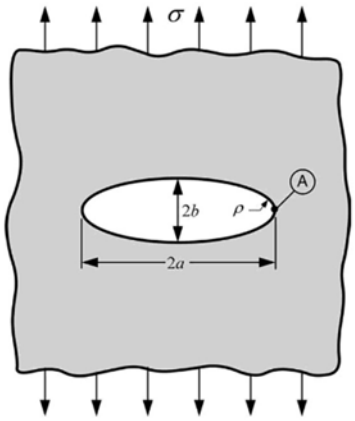

Figure 2 Flat plate with elliptical flaw (Anderson, 2005)

The radius ρ It the crack tip A is given as follows

$$\mathbf{i} = \frac{\mathbf{I}}{} \tag{2.6}$$

Inglis suggested the stress at A to be

$$_{n} = \quad \mathbf{I1} + \frac{\mathbf{I}}{\mathbf{I}} 1 \tag{2.7}$$

Using the definition of the crack tip radius equation (2.7) changes to

$$_{n} = \quad 1 + 2 \quad \frac{}{} \tag{2.8}$$

For a sharp crack tip a >> b and the crack tip radius ρ approaches zero.

$$_{n} = 2 \quad \frac{}{} \tag{2.9}$$

Inglis (1913) was able to prove that equation (2.9) provides adequate description of the stress concentration caused by a crack that is not elliptical when excluding the crack tip. Equation (2.9) results in an infinite stress at the crack tip, where ρ equals zero. However, since the minimum crack tip radius cannot fall below the radius of an atom, ρ can be replaced by xo. If one sets equation (2.9) equal to equation (2.4) the nominal stress at failure can be described by

$$= \frac{\overline{\mathbf{I}}}{} \qquad (2.10)$$

For any radius

$$= \frac{\overline{\mathbf{I}}}{} \qquad (2.11)$$

2.5 Energy Balance and Energy Release Rate

An energy approach as a criterion for crack propagation was first developed by Griffith (1920). According to Griffith, a crack propagates when the external energy, resulting from applied loads, exceeds the internal energy, which is equivalent to the material resistance. The general idea behind Griffith's energy approach is that if a crack grows the contiguous material of the free surface is unloaded and thus its strain energy released. Based on this idea Griffith was able to formulate an equation for a plate with plane stress condition and a width >> the crack length (Figure 3). He expressed the total internal energy U of a cracked plate as

$$= \quad - \quad + \qquad (2.12)$$

Where U_o is the elastic energy of the uncracked plate, U_a is the decrease in elastic energy due to the crack and U_Υ is the increase in elastic surface energy due to the formation of the crack surface. Griffith applied the first law of thermodynamics and found that at instability, when the crack starts

to propagate and the crack surface area increases about dA, the variation in internal energy has to be zero.

$$\frac{}{n} = 0 \qquad (2.13)$$

The elastic energy of the uncracked plate is a constant value and is therefore negligible in the derivation. The elastic energy due to the crack, U_a, and the surface energy, U_Υ, can be expressed as

$$= \frac{}{I}(2I \quad) \qquad (2.14)$$

$$= 2(2I \quad I_n) \qquad (2.15)$$

After deriving equation (2.13) and solving for the stress at fracture the stress at failure can be obtained as

$$= \frac{\overline{II}}{} \qquad (2.16)$$

In 1957, Irwin (Irwin, 1957) proposed a modified version of Giffith's energy approach for fracture that is more applicable to engineering problems. Irwin defined an equation for the rate of change in potential energy with the crack area. The so called energy release rate is defined as (Anderson, 2005)

$$= \frac{}{I} \qquad (2.17)$$

Where σ is the applied stress, a is half of the crack length and E is the Young's modulus. (Anderson, 2005). At fracture, the energy release rate is equal to the critical energy release rate G_c, which is a measurement for the fracture toughness of the material.

$$= \frac{1}{\mathbf{I}} \qquad (2.18)$$

Equation (2.18) describes the important relationship between the material (G_c), the applied stress σ_f, and the critical crack length a_c at failure. Equation (2.18 can be written in a more convenient form

$$\overline{\quad} = \overline{\mathbf{I}} \qquad (2.19)$$

It is important to notice that equation(2.19) can also be obtained by expressing the surface energy $2\Upsilon_s$ at fracture with the fracture toughness G_c in equation (2.16).This shows that Griffith's and Irwin's approaches lead to the same result.

Another important aspect is that the energy release rate is the force causing fracture, while G_c is the material's ability to resist fracture (Anderson, 2005). A fundamental assumption made in fracture mechanics is that the fracture toughness, here G_c, is a size independent material constant. This assumption holds true as long as the material behaves mainly linear elastic (Anderson, 2005).

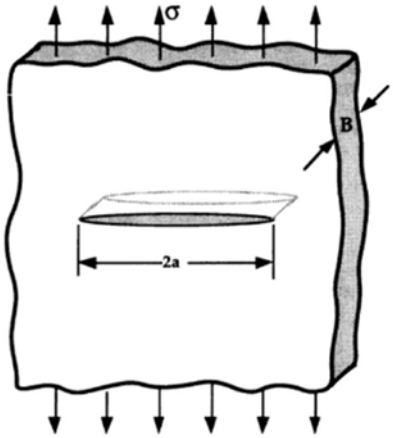

Figure 3 Through thickness crack in an infinite plate subjected to tensile stress (Anderson, 2005)

2.6 Stress Intensity Factor

Irwin's crack intensity approach is an equivalent method to the energy approach developed by Griffith. Irwin managed to characterize the stress field at the tip of a crack with a single parameter, the stress intensity factor. The stress intensity factor is a constant and its subscript identifies the loading modes it is associated with, K_I, K_{II}, and K_{III}. A crack tip can be loaded with either of the three loading modes shown in Figure 4 or a combination of them. Mode 1 is a tensile mode that results in an opening of the crack. Mode 2 and Mode 3 are in-plane and out-of-plane shearing modes, which cause sliding of the crack surfaces relative to each other.

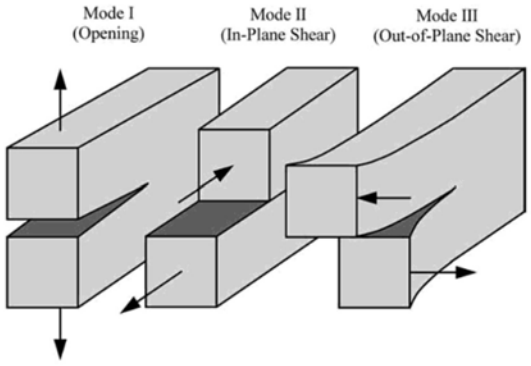

Figure 4 The three modes of loading (Anderson, 2005)

Equations (2.20) through (2.25) describe the stress field for a linear elastic cracked body subjected to mode 1 loading. The equations consist of a leading term and higher order terms. As it can be seen from the equations below if the radius, r, approaches zero the stresses approach infinity, therefore the equations describe a stress singularity. In this region the higher order terms (H.O.T.) become negligible when compared with the leading term.

$$= \frac{I_n}{\sqrt{2}} \cos \frac{}{2} \; 11 - \sin \frac{}{2} \sin \frac{3}{2} n + I \quad + I.\, I.\, I. \tag{2.20}$$

$$= \frac{I_n}{\sqrt{I}} \cos I_I^{-} \; 1\,11 + \sin I_I \; 1 \sin I_I^{I} 1l + \text{H.O.T.} \tag{2.21}$$

$$= \frac{I_n}{\sqrt{2}} \cos \frac{}{2} \sin \frac{}{2} \cos \frac{3}{2} + I.\, I.\, I. \tag{2.22}$$

$$= \quad + \quad \text{(plane strain)} \tag{2.23}$$

$$= 0 \quad \text{(plane stress approximation)} \tag{2.24}$$

Where

r and θ are defined in Figure 5

σ_{ij} = stress tensor

K_I = Stress intensity factor in mode 1

T_{oxx} = T-stress, a constant value that can vary with loading and geometry

H.O.T. = Higher order terms

Figure 5 shows the polar coordinate system with its origin at the crack tip that was used for equation (2.20)through (2.25)

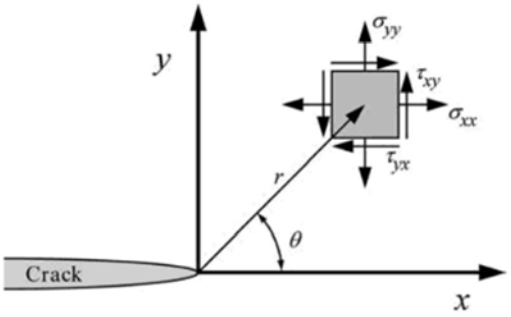

Figure 5 Stresses near the crack tip in an elastic material (Anderson, 2005)

On the crack tip plane where θ = 0 and the shear stresses are zero equation (2.20) and (2.21) become

$$= \quad = \frac{I_n}{\sqrt{I}} \qquad (2.25)$$

Equation (2.25) is only applicable to the area close to the crack tip, where the leading term dominates. Closed-form solutions for some simple solutions have been derived, however for complex problems needs to be solved either numerically or experimentally.

One example for a closed form solution is the through thickness crack in an infinite plate under loading mode I. K is given by

$$I_n = \sqrt{I} \qquad (2.26)$$

It is important to notice the similarities between equation (2.26) and equation (2.19). Comparing these two equation gives the relationship between the energy release rate and the stress intensity factor.

$$I_n = \sqrt{} \qquad (2.27)$$

This relationship suggests that K can also be used to define fracture and fracture occurs when $K = K_{IC}$, the fracture toughness of a material.

2.7 Fatigue Crack Growth

As mentioned previously, fatigue is the process of crack formation and crack propagation in materials subjected to cyclic loading. Crack initiation takes up only a fraction of the total fatigue life; therefore, it is important to incorporate the crack propagation phase when calculating the total fatigue life. Crack propagation is a mechanical process that occurs in a stable manner under service load. The final stage of crack propagation, when the crack is very long, is however unstable. The two most common mechanisms that cause crack growth are fatigue due to cyclic loading and stress corrosion due to sustained loading (Broek, 1989). Following the mechanical process due to fatigue is explained, since this is the one relevant for this thesis.

In fatigue the component is subjected to cyclic loading caused by the subsequent loading and unloading of a structure. During the loading phase the crack is subjected to tension and opens. The opening occurs due to local plastic deformation at the crack tip. The loading is followed by unloading or compression and the crack tip becomes sharp again. In other words, crack growth is a process of repetitive blunting and sharpening of the crack tip. During each loading zone the crack extends about Δa. The crack increment about which the crack opens during each cycle is only in the order of 25 nanometers to 2.5 micrometers (Broek, 1989). However, for structures that are subjected to several millions of load cycles during their life time, such as bridges, Δa easily reaches values that can cause severe damage.

2.8 Paris' Law

In 1963 Paris and Erdogan (Paris & Erdogan, 1963)proposed a model to predict fatigue crack growth. They anticipated that the fatigue crack growth is dictated by the stress intensity range ΔK. The model has the form of a power law, which relates the crack growth rate da/dN to the stress intensity range ΔK. The model is also called the Paris Law and is as follow

$$\frac{}{} = \quad (\Delta I) \qquad (2.28)$$

Where a is half the crack length., N is the number of cycles, C is an experimentally determined coefficient, ΔK is the stress intensity range and m is a material constant. When plotting the Paris Law on a log-log scale it represents a straight line. However, experimental results of da/dN verses ΔK usually do not display in a straight line but have a sigmoid shape on a log-log scale. This is due to the fact that cracks do not propagate for values below ΔK threshold. Therefore, the Paris Law is only applicable to the linear part of the curve.

The accurate prediction of fatigue crack growth using fracture mechanics is a complex task due to a scatter up to a factor of 20 in experimental data for da/dN (H. N. Mahmoud & Dexter, 2005). A lot of the scatter is caused by errors in the experiment but also irregularities in the crack growth rate, especially in the region near ΔK threshold.

It has been shown that the crack growth rate depends on the load ratio, R.

$$R=\frac{}{} \qquad (2.29)$$

However, the Paris Law does not account for this dependence. Several equations exist taking the effect of the load ratio into account. In this study the load effect is accounted for by replacing ΔK by an effective ΔK_{eff} in equation (2.28). Thereby, only the part of ΔK that contributes to the crack

propagation is considered. The basic idea behind this method is that the crack growth model is defined for load ratios greater than 0.7 for which the crack closure can be neglected. If the load ratio is lower than 0.5 or negative, only the part of the load cycle during which the crack is open is accounted for (Mahmoud & Dexter, 2005). The effective stress intensity range is computed by superposition of K_{max}, K_{min} and K_{res}. Where K_{max} is the amplitude of the stress intensity factor associated with the maximum applied load for a certain crack length, K_{min} is the amplitude of the stress intensity factor associated with the minimum applied load for a certain crack length and K_{res} is the amplitude of the stress intensity factor associated with the effect residual stresses for a certain crack length. To apply this method to this study it is assumed that the Paris Law is defined for a load ratio greater than 0.8.

2.9 Probabilistic Analysis

In this study, numerical finite element simulations and probabilistic analysis are combined to account for uncertainties influencing fatigue life. When dealing with engineering problems the engineer is always confronted with numerous unknowns as for example variation in the manufacturing process of the materials, differences in the workmanship, uncertainties in the loading or a combination of all of these. All these uncertainties make it very difficult to accurately predict the behavior of a structure or a structural component in a specific event. Therefore, probabilistic analysis is commonly used to all eventualities in engineering in support of risk-informed decisions.

2.9.1 Monte Carlo Simulation

When predicting the behavior of a structural component or a structure under certain conditions, assumptions are typically made on loading or material properties and are then used in

a deterministic analysis. Those values are usually based on experimental data, experiences or expert knowledge. When conducting probabilistic analysis, uncertainties are accounted for in the simulations so that probabilities of failures can be calculated and decisions are devised based on probabilistic analysis.

Monte Carlo simulation is a computerized mathematical technique that is used in a variety of disciplines such as financing, project management, engineering and research. The method is a popular tool for decision making since it allows the user to determine the probability of failure. A Monte Carlo simulation provides not only a variety of possible outcomes but also the probabilities they will occur.

In a Monte Carlo simulation, each random variable is represented by a probability distribution. In each iteration of the simulation the variable is replaced by a value that is sampled at random from the specified distribution. Using this random value the result is computed and recorded. If this process is repeated a large number (e.g. 1000) of times the output is also a large number of separate and independent results, of which each represents a possible future event. The assembly of all these individual future events represents a probability distribution of possible outcome. The sampling method in a Monte Carlo simulation is entirely random. that means if the input distribution shall be represented accurately a high number of iterations is required since the sampled value can be anywhere within the boundaries of the input distribution.

2.9.2 Latin Hypercube Sampling

Latin Hypercube sampling is a modified sampling method that allows the user to decrease the sampling size compared to that required in a typical Monte Carlo method. Instead of using entirely random samples as in Monte Carlo simulation, the Latin Hypercube method uses controlled sampling. The basic idea is to have the sample point distribution to approach the input

probability distribution as close as possible with the least amount of samples. This is realized by evenly partitioning the sample space into N regions and picking one sample from each region. The sample in each region is random. If N is the number of realization and K is the number of random variables the sample space is K-dimensional and results in a N x K matrix. For a two-dimensional sampling space with five realizations this would result in the sample space shown in Figure 6. The sample space is created by generating a one-dimensional Latin Hypercube samples for the variables X_1 and X_2. Afterwards, the samples are randomly combined to two-dimensional pairs. It is important to notice here that the random variables X_1 and X_2 must be independent.

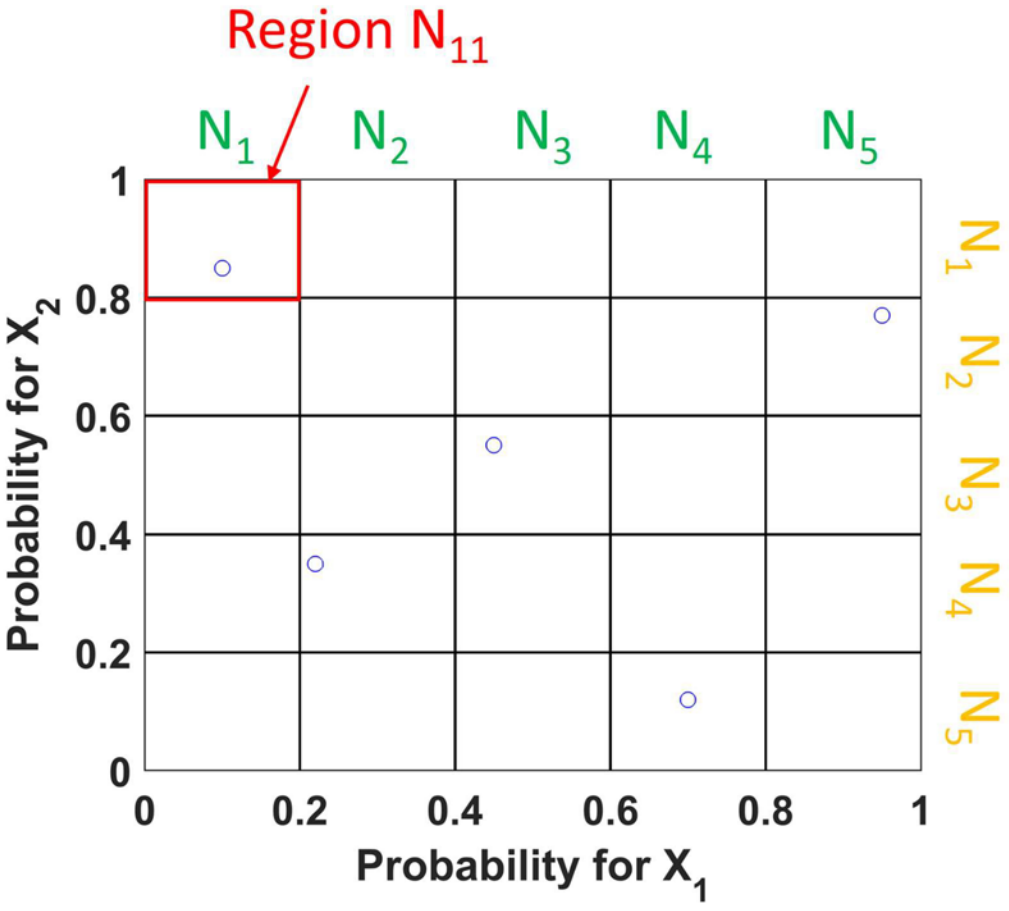

Figure 6 Latin Hypercube sampling for two independent random (X_1, X_2) variable with 5 realizations

2.9.3 Definition of Failure

Structural reliability deals with the ability of structures to withstand loading. There is no uniformly defined quantity that can be used as a measurement of structural reliability, since it depends on the requirements that must be satisfied. There are a lot of different kinds of required performance objectives, depending on the structure type and loading conditions. Those requirements are called limit sates and may be safety against collapse, limitations on damage, or deflections and other criteria (Melchers, 1999). Failure is defined by limit state function, which may be collapse. In Monte Carlo simulation each random variable X_i is sampled at random to give a sample value $\hat{x}_i$. A limit state function $G(\hat{x})$

$$= \quad (\quad \leq \quad) = \quad (\quad - \quad \leq 0) \qquad (2.30)$$

3.1 Bridge Description

The original Betzwood bridge in Montgomery County, Pennsylvania was built in 1964. The Betzwood Bridge is an eight span continuous two-girder steel bridge carrying two lanes of traffic. All spans have an approximate length of 27m and the roadway width is approximately 10m. The superstructure was built with A36 steel and the traffic is carried by a 0.2m reinforced concrete deck. An overall plan and elevation of the Betzwood Bridge is shown in Figure 7 (Daniels et al. 1987).

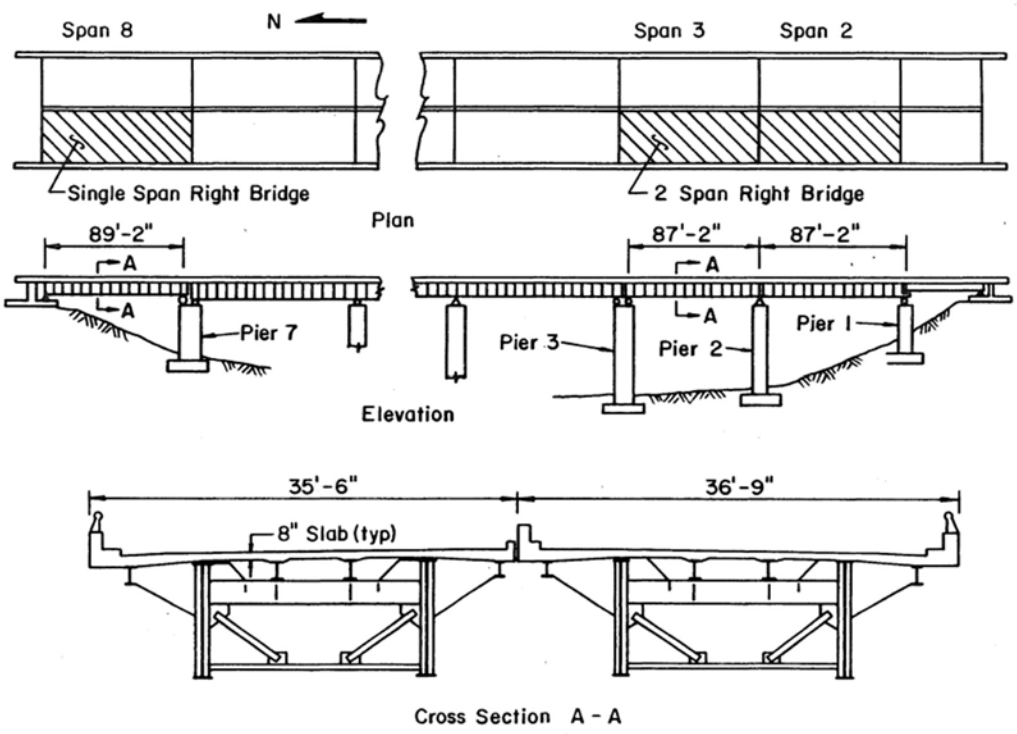

Figure 7 Overall Plan and Elevation of the Betzwood Bridge (Daniels et al., 1987)

For this thesis, span 8 of the original Betzwood Bridge is used to create a numerical simply supported single span two-girder steel bridge model. The span length of the bridge is 27.18m. The

bridge deck is supported by two transversely and longitudinally stiffened girders that are placed with a distance of 5.64m from each other. A detailed view of the girder is shown in Figure 8. The girder is a built up member and its web has a depth of 2.34m with a thickness from 0.01m. The flanges are 0.43m wide and their thickness varies along the girder from 0.05m to 0.04m. The transverse stiffeners have a thickness of 0.01m and are equally spaced at 1.36m (Daniels et al., 1987).

A view of the superstructure below the deck is shown in Figure 9. The deck overhang is supported by the outriggers which are connected to the stringer and the girder. The stringers are wide flange W18x45 sections and are spaced at 1.87m. The floor beams are wide flange W24x84 section. The floor beams, the outriggers and the cross bracing are uniformly spaced at a distance of 5.43m. The bottom laterals are C7x14.75 channels, and the cross bracing are 6x3 1/2x3/8 angles (Daniels et al., 1987).

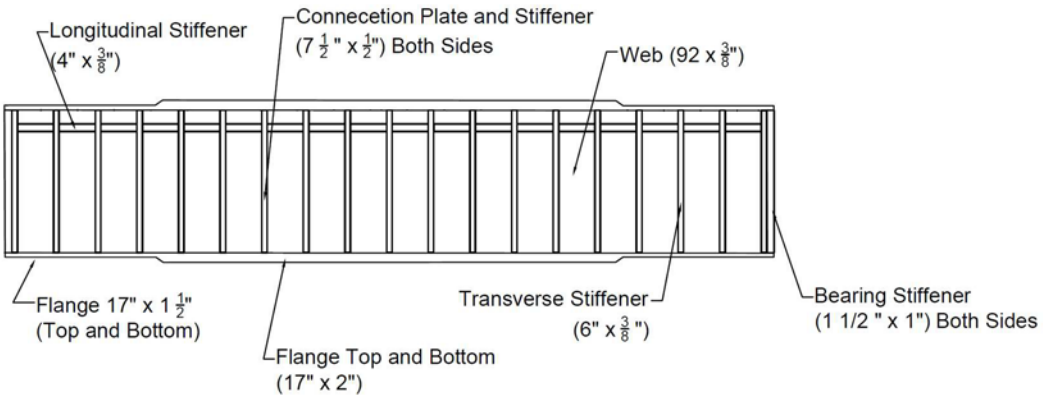

Figure 8 Elevation of girder (after Daniels et al., 1987)

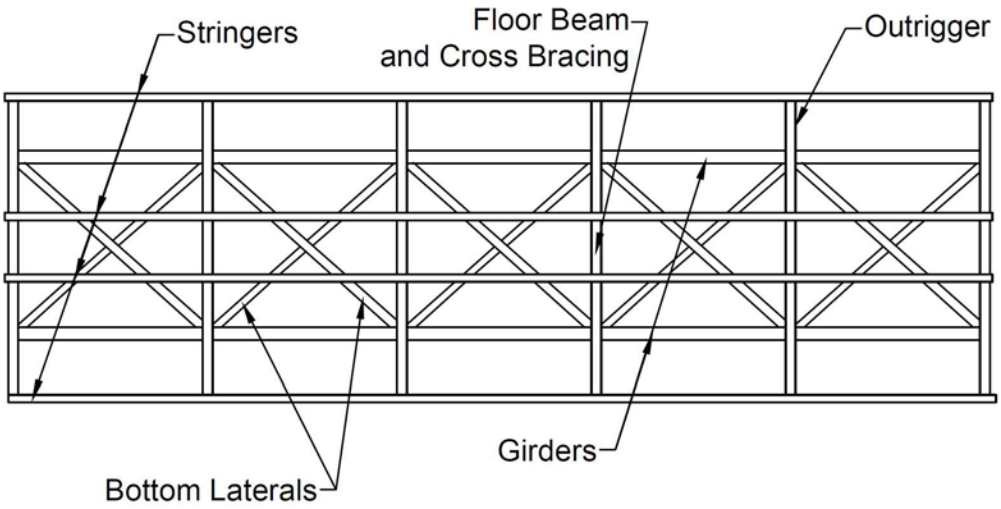

Figure 9 Plan view of superstructure below deck (after Daniels et al., 1987)

The bridge deck has a thickness of 0.2m and is designed of concrete with an ultimate strength of f'_c = 24.13MPa. The flexural strength of the deck is provided by #5 reinforcing bars in the transverse direction. The longitudinal reinforcement is of #4 and #5 bars.

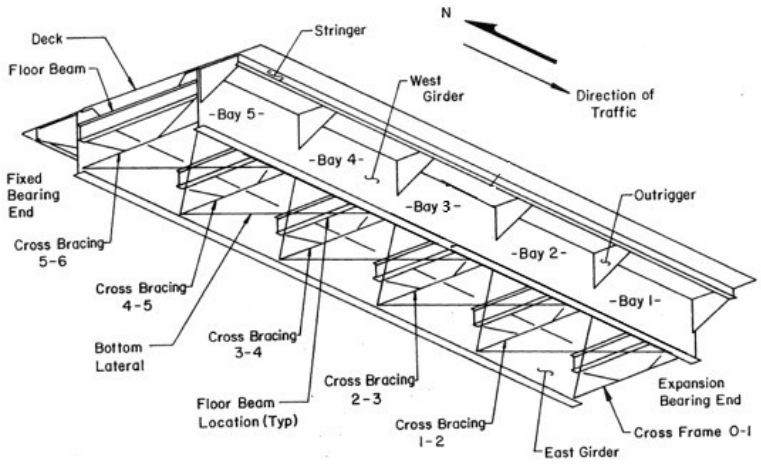

Figure 10 Bridge structure (after Daniels et al., 1987)

3.2 Crack location

As described in the background section in Chapter 2 the number one initiator for cracks are crack-like discontinuities such as bolted and welded connections. As every other bridge, the simple span bridge studied in this thesis has numerous of these crack initiators. The connections between the stringer and the outriggers, the stringers and the girders, the outrigger and the girders and the floor beams are all bolted connections. These mechanical connections are not very susceptible to fatigue. However, the girders are built up members and their flanges and the web are welded. Furthermore, the longitudinal and transverse stiffeners are welded to the girder web. These welded connections influence the fatigue behavior due to residual stresses and flaws. The connection of the bracing system-to-the girder is a combination of riveting and welding. The bottom laterals are riveted to a connection plate that is welded to the bottom flange of the girder. The connection plate detail of the bottom lateral is shown in Figure 11.

The welding of the connection plate and flaws in the weld induce residual stresses and local stress concentrations. Tensile residual stresses are located near the weld and the magnitude usually approaches the yield stress of the material. Since the longitudinal weld is in the direction of the nominal tensile load due to traffic, this detail is very susceptible to fatigue. In the AASHTO manual (AASHTO, 2012) this connection type is defined as a category E' detail and the fatigue threshold is 18MPa. Category E' has the least resistance to fatigue loading and therefore the chance that a crack initiates at the toe of one of the longitudinal welds of the connection plates is very high. Due to that fact, the crack location for this study was chosen to be at cross bracing 3-4 shown in Figure 10.

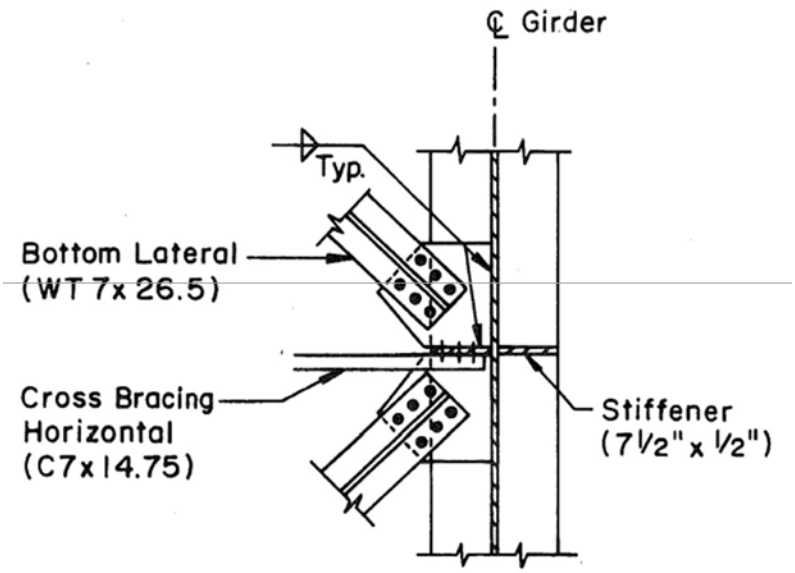

Figure 11 Connection of bottom lateral to grider flange (Daniels et al., 1987)

3.3 Numerical Bridge Model

In this study, a 3D numerical model of a single span two-girder steel bridge is created using the finite element analysis (FEA) software ABAQUS (Abaqus/CAE User's Guide, 2014). ABAQUS is a multipurpose finite element software, which is used in a variety of engineering disciplines. In this study the FEA software is used to run static analyses of stress intensity factors to determine the crack propagation rate. Therefore, the K values are calculated for various crack lengths and compared to the critical value K_{IC} and the crack arrest toughness K_A. K_{IC} is the critical value at which a crack starts propagating in an unstable manner but does not take into account the opportunity that the crack could get arrested due to changing conditions such as the transition into the compression zones. The crack arrest toughness K_A, however, is a dynamic property taking into account the crack propagation velocity and the momentum. If the dynamic toughness is exceeded the crack will not be arrested but propagate all the way through the girder until fracture.

The numerical model is created based on the original Betzwood Bridge described in the previous sections. At first a model without a crack was created. This model was then used as the basis for all further models. In total 34 input decks were created, one without a crack and 33 models with an increasing crack lengths in increments of 0.08m until fracture. Those input decks are the basis for the following reliability analysis. In finite element analyses the computational time depends on the computer power as well as on the model size. Since for the reliability study a high number of analyses had to be run, the difficulty was to keep the model as simple as possible without losing too much accuracy. The overall model setup and the simplifications made for the numerical model are explained in the following paragraphs.

3.3.1 Geometry

The geometry and the dimensions are obtained from the descriptions and drawings provided in the work by Daniel et al. (1987). For organizational purposes each bridge element was first modeled as an individual part in ABAQUS, so that the designer can assign different section properties such as thickness and material to each part. Afterwards the individual parts, e.g. flange and web, were assembled to one component, e.g. the girder. Using this technique, the whole bridge model finally consisted only of seven assemblies (deck, girders, floor beams, stringers, outriggers, lateral bracing and cross bracing). A view of the bridge structure is shown in Figure 12.

As described previously, the traffic is carried by a reinforced concrete deck. Modelling the concrete deck and the embedded reinforcing bars realistically would be very time consuming, since it is complicated to simulate the interaction between the individual components in contact. For this reason, the reinforced concrete deck is simplified as a simple two-dimensional plate with a certain thickness and the properties of the steel and the concrete are combined in the material definition.

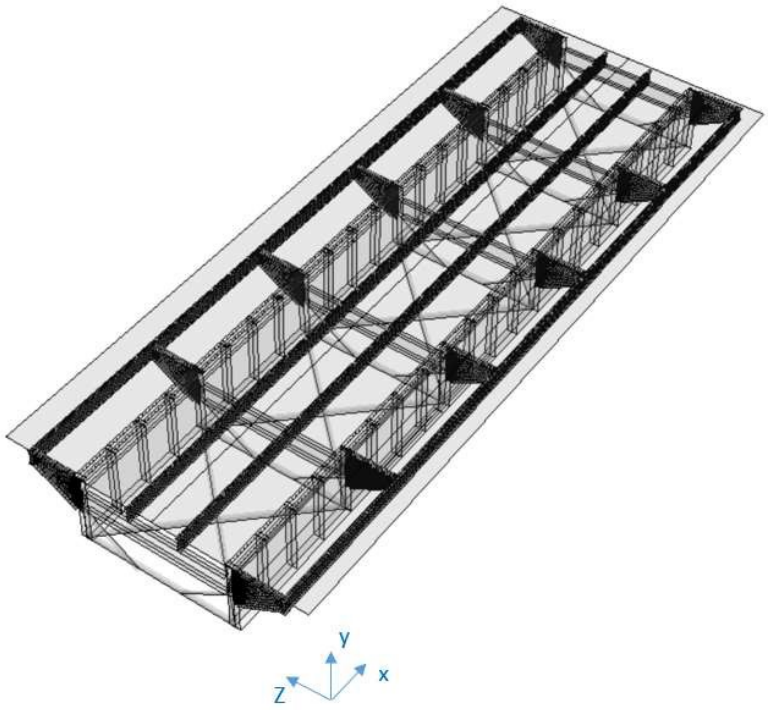

Figure 12 Bridge structure

3.3.2 Material

ABAQUS provides an extensive material library that allows the user to model most engineering materials. In this study only two different materials need to be defined, steel and reinforced concrete. Since linear elastic fracture mechanics is conducted, only the linear elastic part of the material curve needs to be defined for the analyses. The material card for elastic materials available in ABAQUS requires entries for the Young's modulus and the poisson's ratio. The material parameters defined in the numerical model are listed in Table 2. As mentioned above the reinforced concrete deck is simplified and the steel reinforcement is not modeled. Hence for the material of the deck an effective Young's modulus for the steel and concrete. The effective Young's modulus for the reinforced concrete is calculated based on the work by (Norita, 1985)

Table 2 Material Properties defined in the numerical model

Material	Young's modulus	Poisson's ratio
Steel	200MPa	0.3
Reinforced concrete	25.6558MPa	0.3

3.3.3 Model Mesh

The three-dimensional model of the bridge consists of 2D shell elements and 1D beam elements. The main structural components (bridge deck, girders, floor beams, outriggers and stringers) are modeled using four and three nodes shell elements. The element types specified in ABAQUS are S4R and S3R, respectively. Where the S stand for shell, the number corresponds to the number of nodes and the R stands for reduced integration. The reduced integration element type was chosen to save computation time. In FEA numerical integration is used to compute the element stiffness and mass. ABAQUS uses the Gaussian integration method to calculate the element matrices. Using elements with a reduced integration method safes time because less integration points are used when computing the element matrices.

The bottom laterals, the cross bracings, and the shear studs are model with 1D beam elements. The approximation of a 3D structure with a 1D element is possible because the cross-section is small compared to its longitudinal dimensions. In ABAQUS beams are modeled by line elements. The cross-section is then defined by a profile which is assigned to the part in the section module. A section of the meshed bridge model, the beam profiles and the bracing system is shown in Figure 13.

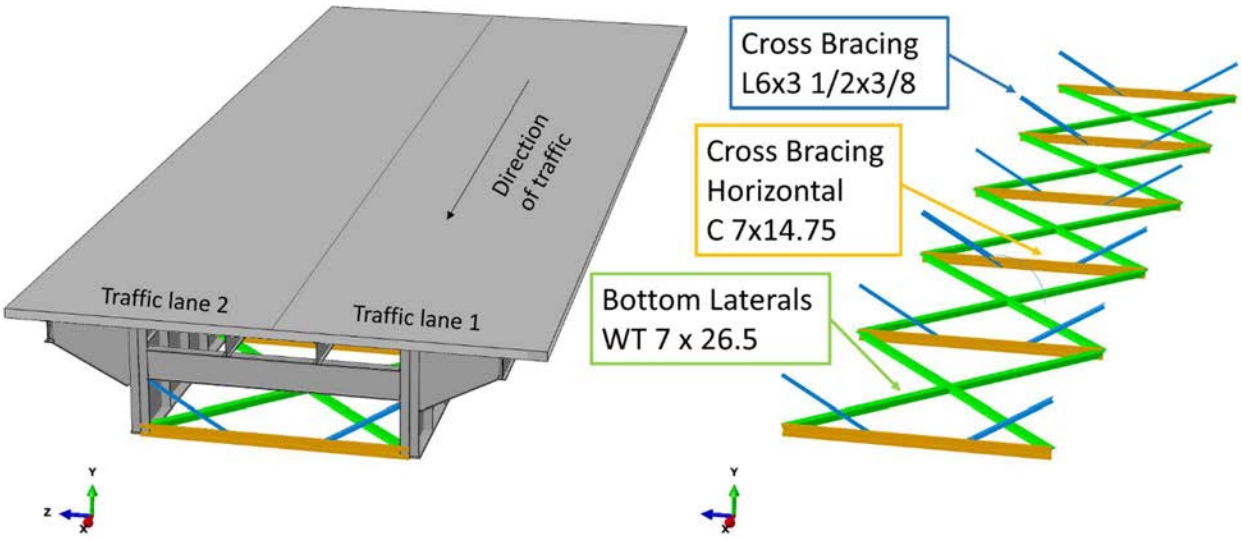

Figure 13 Bridge structure with bracing system (left) and isolated bracing system and beam profiles (right)

3.3.4 Boundary Conditions

The original Betzwood Bridge is an eight span continuous two-girder steel bridge. However, in this thesis only a single span of the structure is considered, which means that the boundary condition changes. The single span is simply supported by a pin on one end and a roller on the other end. These boundary conditions are implemented in the ABAQUS model by locking the desired degree of freedom (DOF). The orientation of the bridge model can be seen in Figure 12. The roller is defined by locking all DOF except the translation along the x-axis and the rotation about the z-axis. The pin is defined by locking all DOF except the rotation about the z-axis.

3.3.5 Connections

The bridge has three different types of connections, bolted, riveted and welded. These connections are implemented in the numerical model by tie constraints. A tie constraint is defined by a master and a slave set that will be tied together during the simulation. The sets can either be

defined based on geometry such as surfaces and edges or based on the mesh. In this work the master surface was chosen to be the component with the coarser mesh and the slave surface was chosen to be the surface with the finer mesh. This is a typical method to avoid conflicts in the algorithm that searches for the slave nodes in a predefined distance to the master node and ties them together.

Using a tie contact to model a bolted or riveted connection, instead of modeling the actual bolt or rivet, simplifies the interaction between the connected components drastically. However, this is acceptable since the focus in this study is on the fatigue behavior which is not directly influenced by this simplification. Nevertheless, the connections influence the load transfer and therefore the connected area was limited to the area representing the bolt. For this reason, circular sections with the diameter of the bolt hole were partitioned and only these areas were part of the contact definition. Figure 14 shows the bolted connection between the girder (black) and the floor beam (blue).

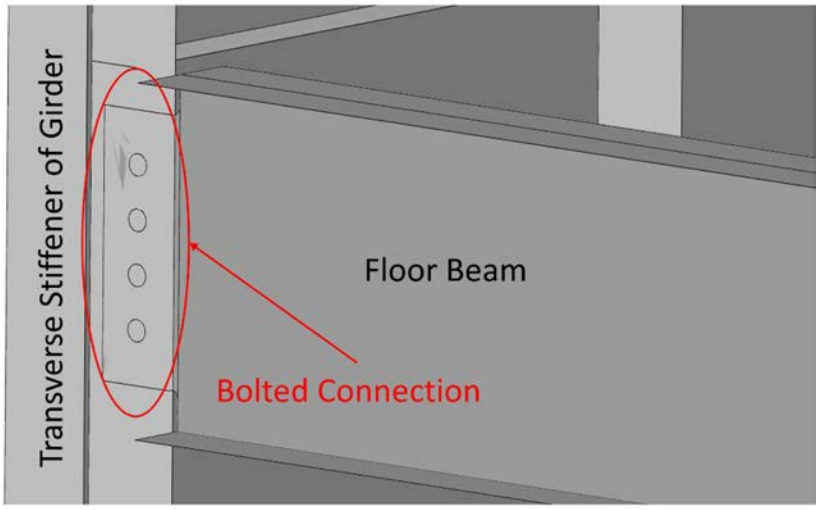

Figure 14 Bolted connection connecting floor beam to girder

3.3.6 Residual stresses

As mentioned in Section 3.2 the crack location for this study was chosen at a connection detail with fatigue category E'. One of the major reason, that this connection is a fatigue category E' detail are the residual stresses due to welding. The influence of residual stress on the fatigue behavior is not negligible and therefore it has to be considered in the FEA. ABAQUS offers an option to define so called predefined stress fields. This option is used to implement residual stresses in the finite element model.

The size of the tension area next to the toe of the weld is computed in accordance with the Faulkner model. Faulkner (1975) suggests a region for the tensile stresses of $\eta * t_{plate}$. Where t is the thickness and η is a value between 3.5 and 6. Here a value of 4 was chosen for η. Figure 15 shows the separated area on the flange and the web, where the residual stresses were applied. The stresses are only in the region where they have an influence on the crack propagation. The stresses have a magnitude of 248MPa, which is equal to the yield stress of the material and are applied in the σ_{11} direction.

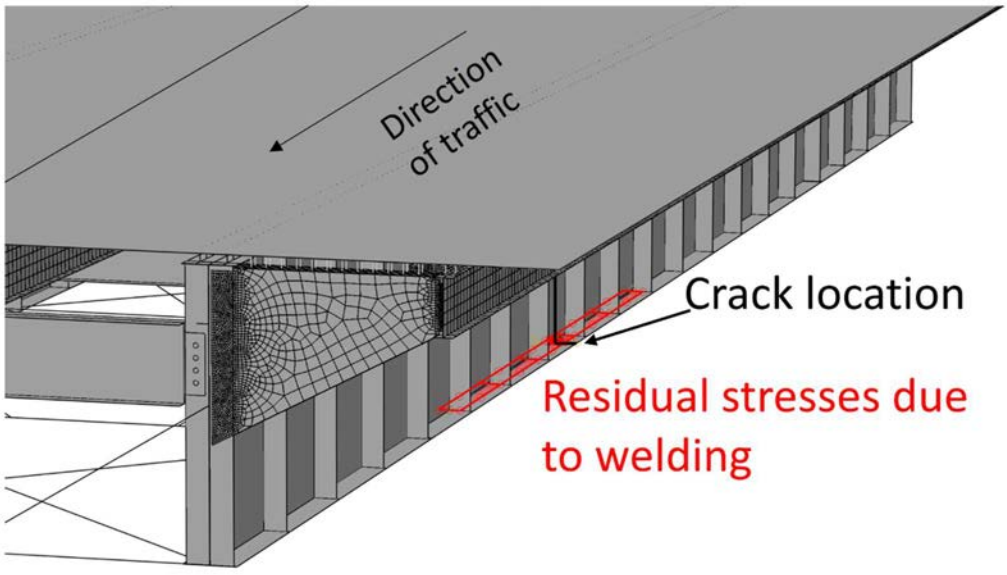

Figure 15 Residual stresses resulting from welding

3.3.7 Loading

The loading for the fatigue limit state is defined in the AASHTO LRFD Bridge Design Specification (AASHTO, 2012). For fatigue a single design truck, equivalent to variable amplitude loading, with a fixed rear axle spacing of 9.144m (30ft) is placed along the bridge to produce the worst case scenario. The steering axle weight is 55.16MPa and the first and second rear axle group weight is 220.63MPs. The weight and axle spacing in units of ft and kips, as specified in AASHTO, is shown in Figure 16.

The axle weight is uniformly distributed over the tire contact area of two tires for the steering axle and four tires for the rear axles, respectively. The exact tire dimensions and placement is as shown in Figure 17. The truck is located at the center of the traffic lane directly over the crack location to simulate the worst case scenario. In ABAQUS the tire contact areas are modeled as plates meshed with shell elements. The axle weight is converted to a pressure and applied to the plates representing the tires. A general contact defined between the reinforced concrete deck and the tires is used to allow the load to be transferred.

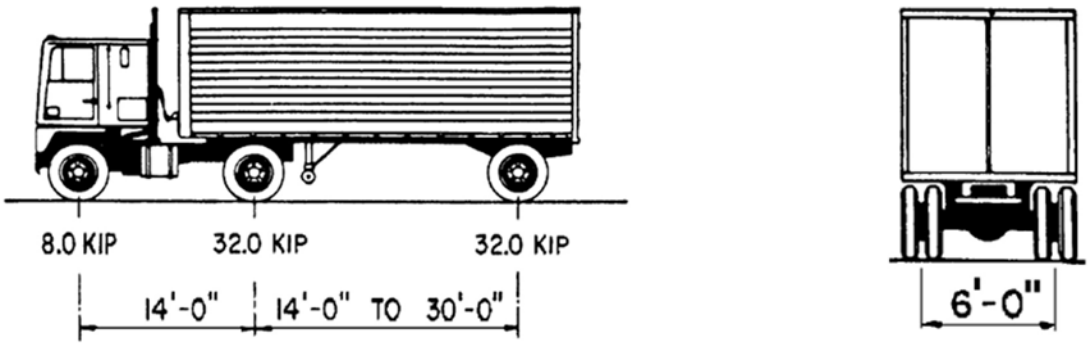

Figure 16 AASHTO design truck (AASHTO, 2012)

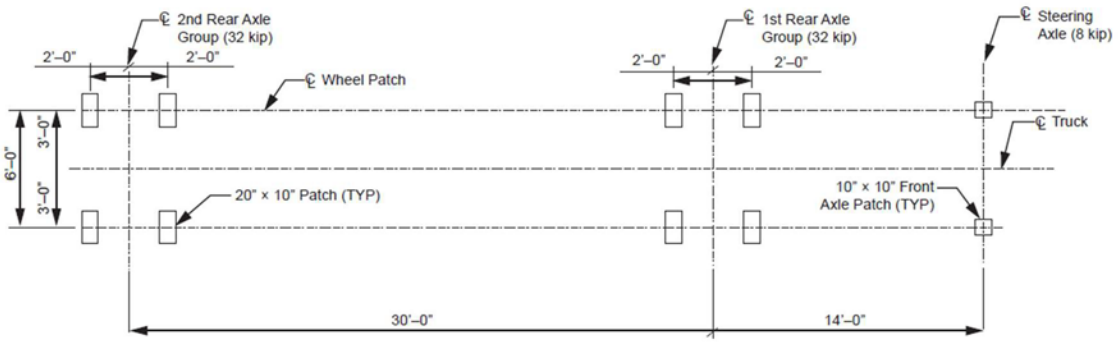

Figure 17 Footprint of the fatigue design truck (AASHTO, 2012)

The implementation of the truck load in the numerical model is shown in Figure 18.

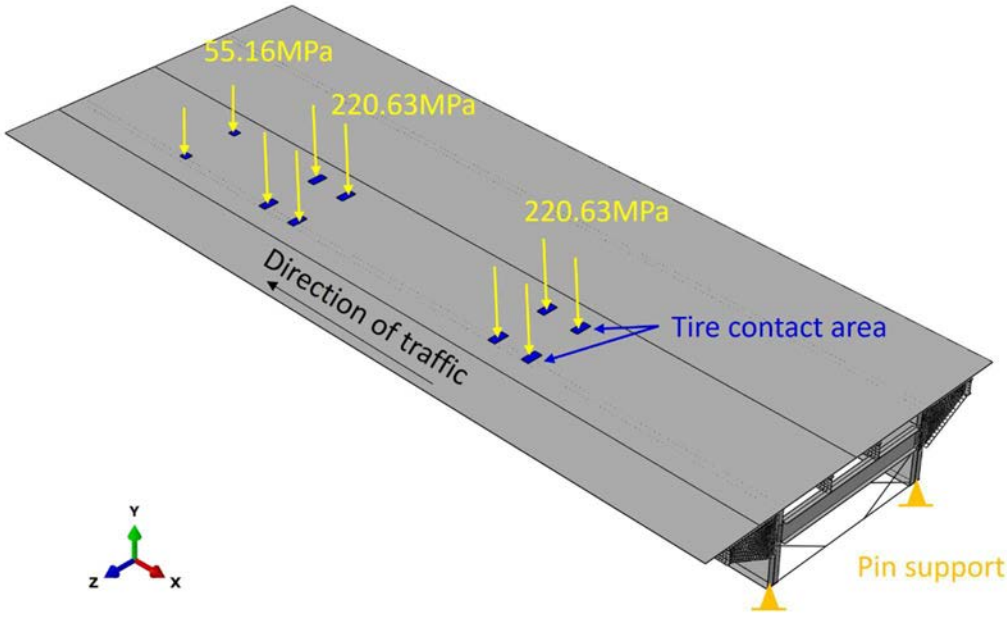

Figure 18 Implementation of truck load in the numerical model

Besides the design truck, AASHTO also defines a Dynamic Load Allowance (IM). The IM is given in percentages and an amplification factor has to be calculated by 1+(IM/100) (AASHTO, 2012). This amplification factor is then applied to the design truck to increase the static load effects. By applying the IM to the fatigue truck, dynamic effects caused by the impact from moving

vehicles are taken into account. These dynamic effects are caused by the dynamic response of the bridge to the moving vehicles and by hammering effects, which is the dynamic response of the wheel assembly to discontinuities in the road. In bridges those could be deck joints, potholes, cracks or delamination (AASHTO, 2012). The IM is not directly applied in the ABAQUS model but is later considered as a random variable when conducting the Monte Carlo simulation.

For evaluating the redundancy, the bridge is subjected to the maximum design load as defined in AASHTO (2012). The maximum design load includes the lane load plus the design truck and the applicable amplification factors. The number of design lanes that need to be applied is computed by dividing the clear roadway width by12ft. For the Betzwood Bridge this results in two lane loads of each 3.1kPa applied in a 3.05m design lane. The design truck for the maximum design load is the same as for the fatigue load case, however, the rear axle spacing is variable between 4.3m and 9m. The axle spacing chosen must present the critical load effect. For a simple span bridge, the critical load effect is caused by a rear axle spacing of 4.3m. The amplification factors applicable for the loading scenario in this study are the load factor for live load and dead load, the multiple presence factor and the dynamic load allowance. The values used for this study are listed in Table 3 and the implementation in the numerical model is shown in Figure 19

Table 3 Load amplification factors for maximum design load

Amplification factor	value
Live load	1.75
Dead load	1.5
Multiple presence factor	1
Dynamic load allowance	1.13

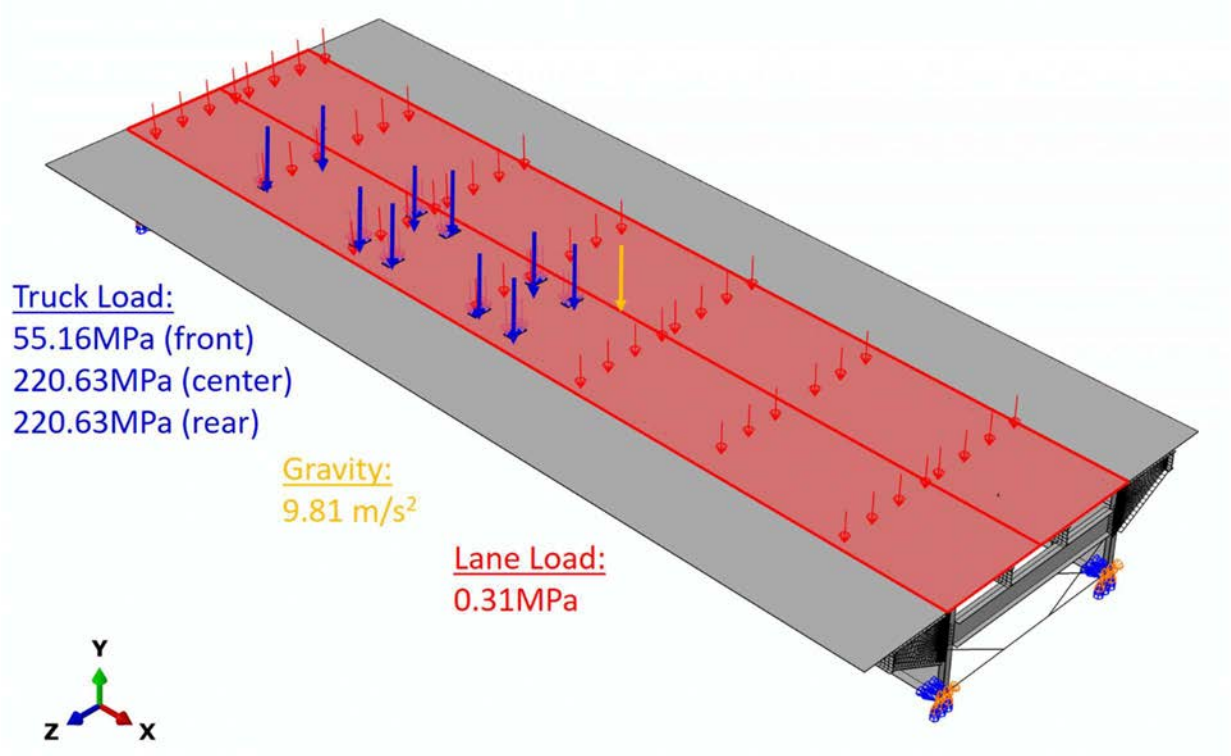

Figure 19 Maximum Design Load

3.3.8 Crack

ABAQUS provides several methods to calculate cracks (Abaqus/CAE User's Guide, 2014). The extended finite element method (XFEM) is the most complex of the methods. It allows the user to simulate crack initiation and propagation along an arbitrary, solution-dependent path without remeshing. Another method is the virtual crack closure technique (VCCT). This method enables the user to study crack initiation and propagation along a predefined surface. The third method and the one used in this study is the contour integral estimate. This option allows to study the beginning of cracking in quasi-static problems.

The contour integral is an output quantity and does not have any influence on the results (Abaqus/CAE User's Guide, 2014). The contour integral option in ABAQUS can be used to compute several output variables relevant in fracture mechanics, e.g. the J-Integral, the crack

propagation direction or the stress intensity factor. In this study the contour integral is used to compute the stress intensity factors for various crack lengths. A contour is a ring of elements completely surrounding the crack tip from one crack face to the other. ABAQUS automatically finds these elements during the analysis but the user can choose the number of contours (rings of elements) that should be evaluated. Since a contour is a ring of elements, the mesh at the crack tip has to be relatively detailed for an accurate evaluation. Also the crack tip and the crack extension direction have to be defined for the calculation of the contour integral. A visualization of the contour integral at the crack tip can be seen in Figure 20.

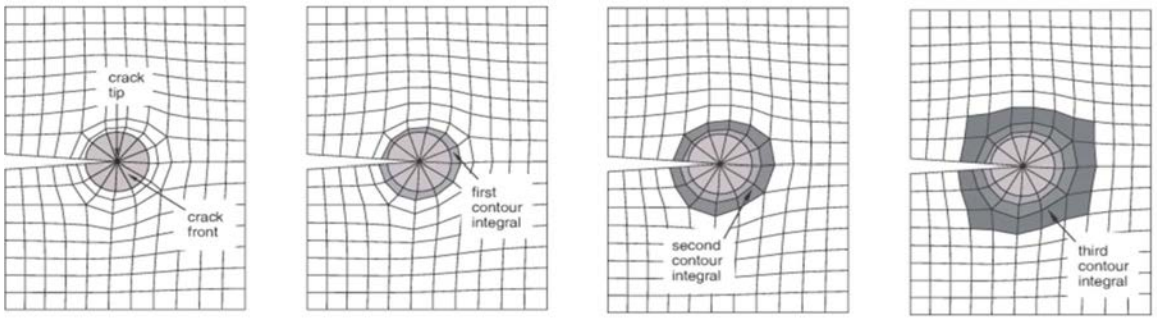

Figure 20 Visualization of a contour integral (Abaqus/CAE User's Guide, 2014)

The contour integral method does not provide the option to predict crack propagation. Hence the crack path was predefined and the crack was opened manually. The crack was propagated in increments of 0.08m starting at the bottom flange, growing into the web all the way up to the top flange. Since the crack is imbedded in the flange and web surfaces the crack had to be defined as a seam crack. For this reason, the girder flange and web were partitioned into 0.08m long increments at the location where the crack is propagated. A seam could then be defined for each individual crack length. When meshing a part containing a seam, ABAQUS creates two independent overlapping nodes along the seam that can move apart when the crack opens during

the analysis. Figure 21 shows the crack location, the crack definition and the crack opening after the analysis.

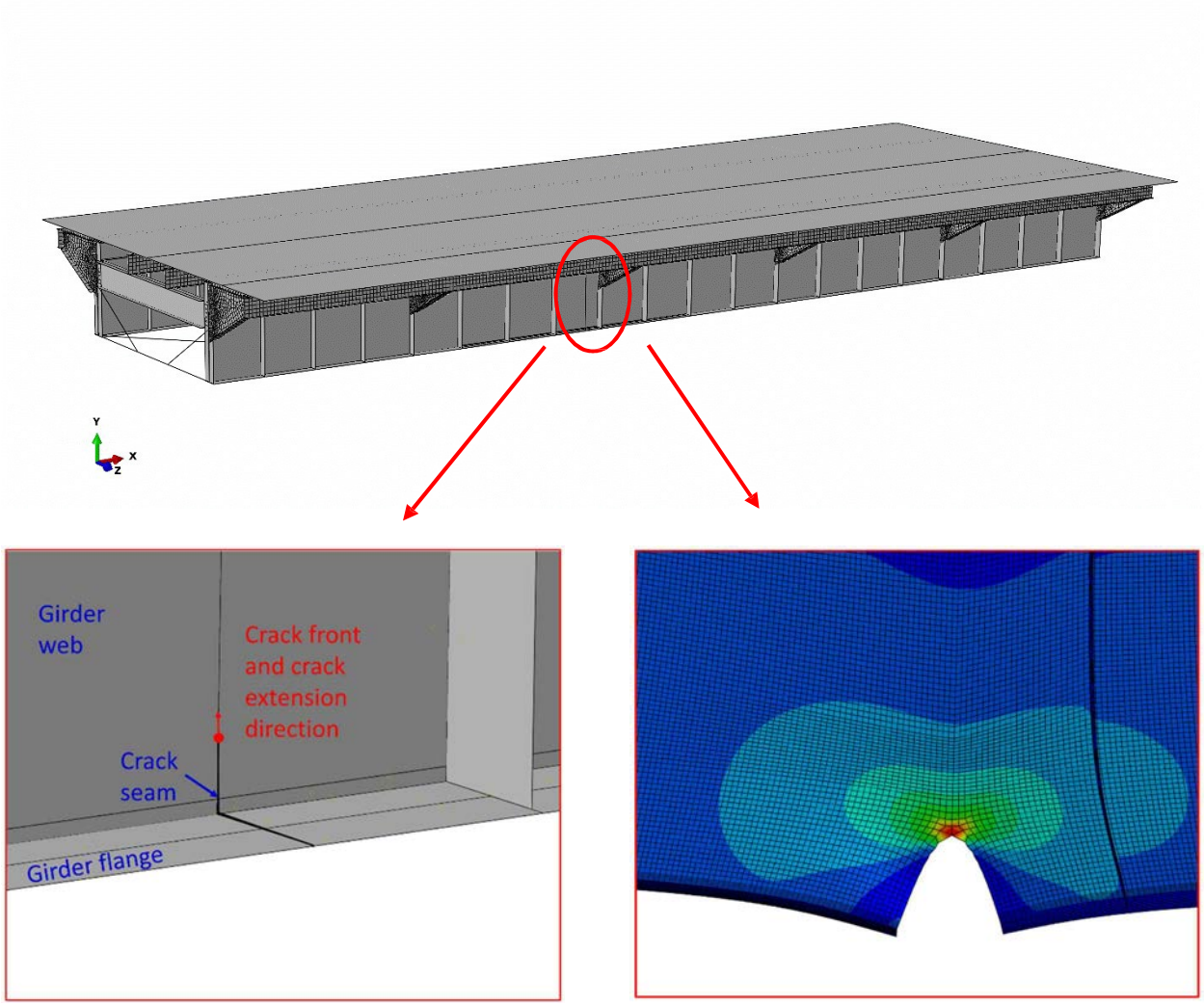

Figure 21 Crack definition in ABAQUS

SIMULATION METHODOLOGY

The input files, which are text files, created by ABAQUS serve as the basis for the reliability analysis and the redundancy evaluation. The reliability analysis was conducted using MATLAB as a programming tool. A program was written to automatize the process of modifying the input file and running the ABAQUS simulations. This is very convenient because MATLAB provides a built in function that sends a command to ABAQUS to run the input file. In the next sections the individual steps of the reliability analysis are outlined. An overview of the reliability assessment process of the bridge is presented in Figure 23, which builds off the work conducted by Mahmoud and Riveros (2014).

4.1 Finite Element Analysis

In the previous chapter the setup of the numerical bridge model was described. This model is the basis for all further FEA. For the study of the fatigue behavior of the bridge three different simulations were conducted.

- At first, the intact bridge model, without a crack, subjected to fatigue loading was simulated. The stress in σ_{11} direction is evaluated at the location, at which in subsequent simulations the crack will be initiated.
- Afterwards the model was used to calculate the stress intensity factor for each crack length that it takes for the crack to travel through the girder in 0.08m increments until fracture. In each analysis the output of five contour integrals was requested. The K value was computed by averaging the second through the fifth contour integral. The value closest to the crack tip was neglected since it is not very accurate due to the singularities

at the crack tip. The output of these analyses correspond to the applied stress intensity factor, $K_{applied}$.

- Finally, the influence of residual stresses on the stress intensity factor was examined. For this reason, the fatigue crack was removed and the residual stresses of the magnitude of σ_{yield} were applied. Again, the stress intensity factor for each crack length that it takes for the crack to travel through the girder in 0.08m increments until fracture, was calculated. The output of these analyses was K_{res}.

Overall ABAQUS was used to create 67 input files for the reliability analysis. One input file for the analysis of the stress in σ_{11} direction. Thirty-three models of the bridge subjected to fatigue loading of which each contains a crack of different crack length and 33 models of the bridge with residual stresses of which each contains a crack of different crack length.

Subsequent, to the reliability analysis the structure's redundancy is evaluated. For this purpose, a separate bridge model subjected to the maximum design load, which is described in the previous chapter was utilized. After the FEA the stresses and the equivalent plastic strain are evaluated and compare to the yield strength and the failure strain for grade A36 steel.

4.2 Monte Carlo simulation

4.2.1 Random Variables

The first step in the Monte Carlo simulation is to define the random variables to be varied during the FEA. It is essential to pick the varying parameter so that they affect the output variable of interest. The final output variable considered after the FEA was the stress intensity factor K. As explained in chapter 2 the stress intensity factor is defined as

$$I_n = \sqrt{I} \qquad (4.1)$$

Considering equation (4.1) it is obvious that the crack length and the stress are the two variables directly influencing K. For this study it was decided that the stress should be the varying quantity. The direct correlation between the stress and the Young's modulus by

$$= \qquad (4.2)$$

and the stress and the applied load by

$$\overline{\overline{n}} \qquad (4.3)$$

Those correlations ((4.2) and (4.3)) suggest to use E and M as random variables. The random variables in a Monte Carlo simulation are described by statistical distributions. Various previous studies incorporating statistical distribution of steel properties have utilized a Gaussian normal distribution with a mean of $1.05F_y$ and a coefficient of variation of 0.1 for the Young's modulus based on the work by Galambos & Ravindra (1978). The fatigue load defined in the AASHTO design specification is a combination of the fatigue truck and the dynamic load allowance (IM). Since the IM can be converted into an amplification factor it is convenient to choose it as the varying quantity for the load. The distribution is Gaussian normal with a mean of 1.13 and a coefficient of variation of 0.1. The statistical distribution was chosen in accordance with Nowak (1995). A summary of the statistical distribution used for Young's modulus and dynamic amplification factor are listed in Table 4.

The random variables are changed for every single stress intensity factor simulation. Thereby it is ensured that the created data can represent any bridge, in any condition, at any location. This is important so that the final results are representative for all two-girder steel bridges and at the same time it ensures the applicability of the results to any two-girder steel in bridge.

Table 4 Statistical distributions used in Monte Carlo simulation for Young's Modulus and dynamic amplification factor

Random Variable	Distribution	Mean	COV	Reference
Young's modulus	normal	$1.05F_y$	0.1	(Galambos & Ravindra, 1978)
Dynamic amplification factor	normal	1.13	0.1	(Nowak, 1995)

4.2.2 MATLAB Program

After the statistical distributions for the random variables were defined, a MATLAB program was written to automatize the process of modifying the input file and running the ABAQUS simulations. MATLAB was used to create random numbers with Gaussian normal distribution for the load and the Young's modulus. Afterwards MATLAB opens and reads the ABAQUS input file and copies the information into a new input file while changing the load and the Young's modulus using the random variables created before. This new ABAQUS input file was then used to run the finite element analysis with the modified load and Young's modulus. At the end of each analysis ABAQUS writes the requested output into a *.dat file, which then can be read again by MATLAB. This process was coded in a loop and can be repeated as often as desired. The sequence of these steps is visualized in Figure 22.

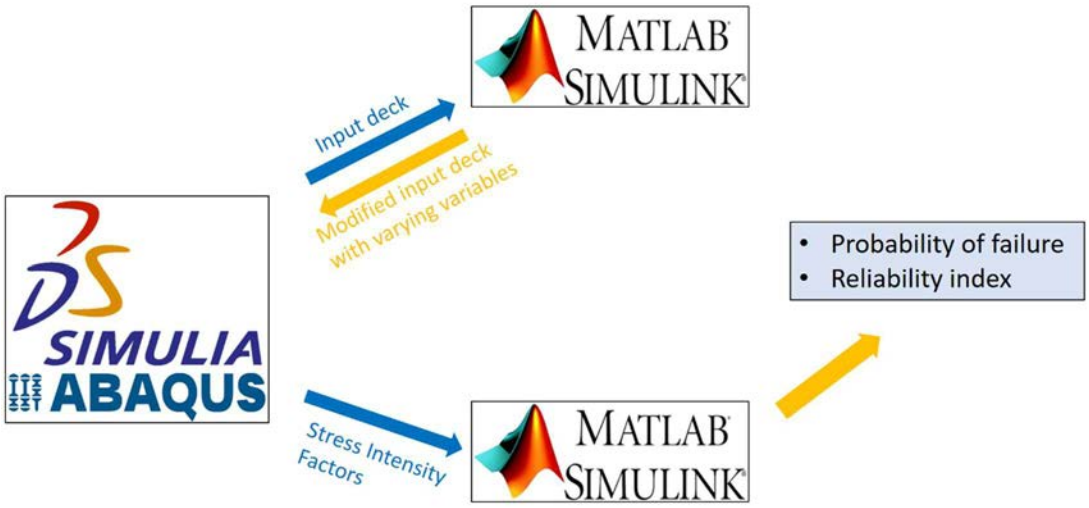

Figure 22 Sequence in reliability analysis (phimeca, 2016)

4.2.3 Number of Iterations for Monte Carlo simulation

The next step was to determine the number of iterations for the Monte Carlo simulation. As explained in Chapter 2 Latin Hypercube Sampling allows to decrease the required number of iterations by using controlled sampling for the random variables. The minimum required number of iterations for accurate results was found by running the above described MATLAB code 3 times with 30, 50 and 75 iterations. The requested output variable were the σ_{11} stresses. ABAQUS computes those in each of the iterations. Afterwards the mean values were calculated for the 30, 50 and 70 values of σ_{11}, respectively and compared with each other. If the mean values for two Monte Carlo simulations are within a small tolerance, the smaller number of iteration is sufficient for accurate results.

4.2.4 Statistical Computation of K

The previously described MATLAB code was modified to run statistical analyses of the stress intensity factor. The sequence of the individual steps remains the same however the output

variable was changed to the stress intensity factor, K. The code was modified so that MATLAB reads the five contour integrals computed during the simulation from the ABAQUS output file. The average of the values is calculated and the results are written into an Excel document. Using the same statistical distributions and random variables as before 50 K values for each crack length are calculated. In total, the analysis is conducted for 33 crack lengths, which resulted in 1,650 K values. The same code is used to determine the stress intensity factor for the third numerical model containing the residual stress. The final output is as well an Excel document containing 50 K values for each crack lengths.

4.2.5 Statistical Computation of the Number of Cycles

After the stress intensity factors were evaluated the Paris' Law was applied to calculate the number of cycles needed to propagate the crack an increment da. As explained in Chapter 2, the stress intensity factor range ΔK in the Paris' Law, equation (2.28), is replaced by ΔKeff, to account for the effect of load ratio. ΔKeff is obtained by superposition of Kmin, Kmax and Kres, which were obtained by running each load case separately. Since the bridge is simply supported, Kmin was taken as zero since the minimum load of zero is represented with the complete passage of the truck over the bridge. The number of cycles were calculated using the results for K evaluated in the FEA in which the load and the Young's modulus were varied. Additionally, statistical crack propagation parameters for the material constant m and the coefficient C were used. In reference to British Standards (1997) a Gaussian normal distribution with a mean of 16.5e-12 MPa(m)1/2 and a coefficient of variation of 0.06 was used for C. Similarly, a Gaussian normal distribution with a mean of 3 and a coefficient of variation of 0.03 was applied for m. An overview of the statistical distributions used in this study is given in Table 5. The number of iterations for the

Monte Carlo simulation was 10,000. That means for each of the 1,650 stress intensity factors 10,000 corresponding number of cycles were calculate.

Table 5 Statistical distributions used in Monte Carlo simulation for the Paris' Law parameters

Random Variable	Distribution	Mean	COV
coefficient, C	normal	9.0e-12	0.06
Material constant, m	normal	3.0	0.01

4.2.6 Probability of failure

The overall goal of this study is to provide the probability of failure with respect to the inspection interval, on the basis of which a sufficient inspection interval can be chosen for a desired probability of failure. Therefore, the number of cycles calculated with the Paris Law are compared to the number of cycles in which the bridge is inspected. If the calculated number of cycles to failure exceeds the number of cycles per inspection interval the bridge fails. The probability of failure is calculated using

$$= \quad < 0 \qquad (4.4)$$

Where g(x) is the objective function and p[g<0] is the probability of the g(x) being less than zero. The objective function is defined as

$$( ) = \quad - \qquad (4.5)$$

Where N_f is the number of cycles to failure and is evaluated using the Paris' Law

$$= \mathbf{I} \qquad (4.6)$$

$$\frac{}{1 \quad \Delta \mathrm{I}^{\mathbf{1}}}$$

Where N_i is the selected inspection interval, a_i and a_f are the initial and the final crack length, m is a material constant and C is a coefficient which is determined experimentally. A schematic presentation of the reliability assessment process of the bridge is shown in Figure 23 (Mahmoud and Riveros, 2014).

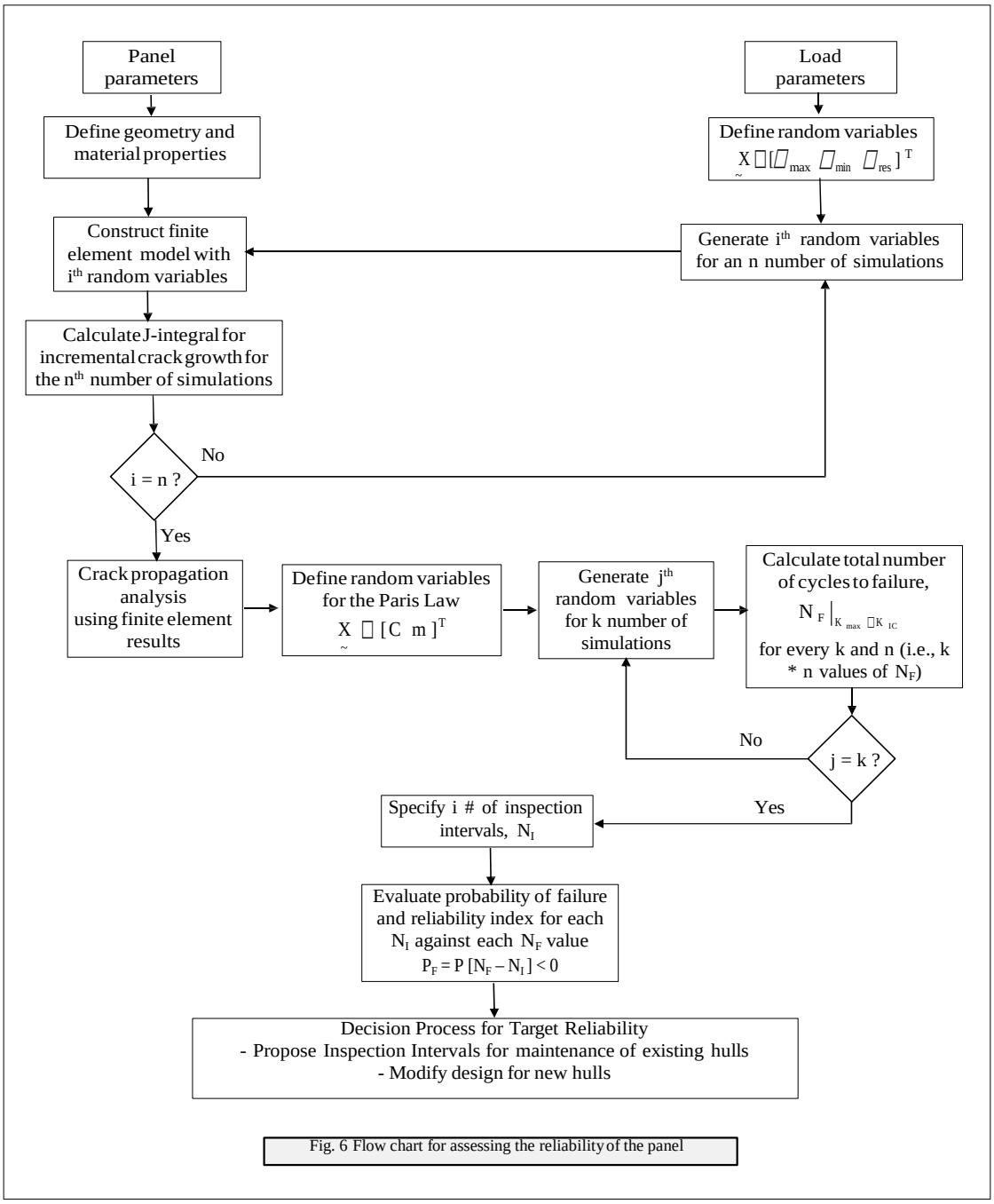

Fig. 6 Flow chart for assessing the reliability of the panel

Figure 23 Process of reliability assessment of the bridge (Mahmoud and Riveros 2014)

RESULTS

5.1 Global System Response

The global system response of the bridge subjected to the fatigue truck loading, which is placed in the center of the right traffic lane directly over the detail in question, is shown in Figure 24 through Figure 27. The plots are all amplified with a factor of 300 for better visualization.

Figure 24 displays three different views of the uncracked bridge displacement in the vertical direction. It can be seen that the girder directly underneath the fatigue truck bends more than the girder that is not directly under the applied load. This was expected due to the asymmetric loading. Furthermore, the asymmetric loading leads to a rotation of the structure about the x-axis, which results in distortion (Figure 24). This distortion causes the girder to move out of the xy-plane and leads to local stress concentrations at the bolted connections of the floor beams to the girders. The von Mises stress distribution for the bridge without crack loaded with the fatigue truck is displayed in Figure 25. The maximum resulting stress is 54.21 MPa occurring at the pin support closest to the fatigue category E' detail (front right in Figure 25). The stresses in the region close to the critical location are about 18MPa.

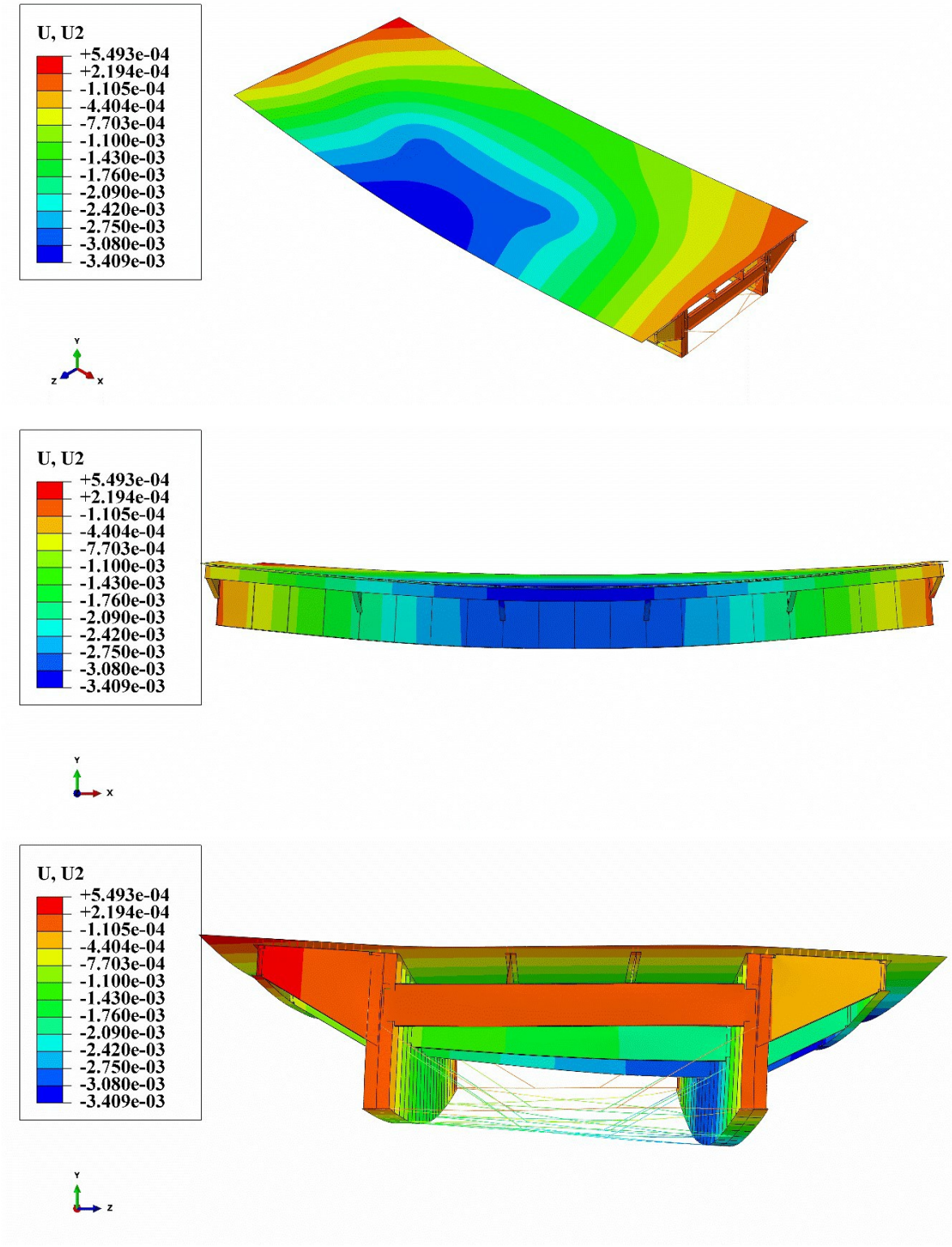

Figure 24 Global deformation in vertical direction of uncracked bridge (amplified by 300)

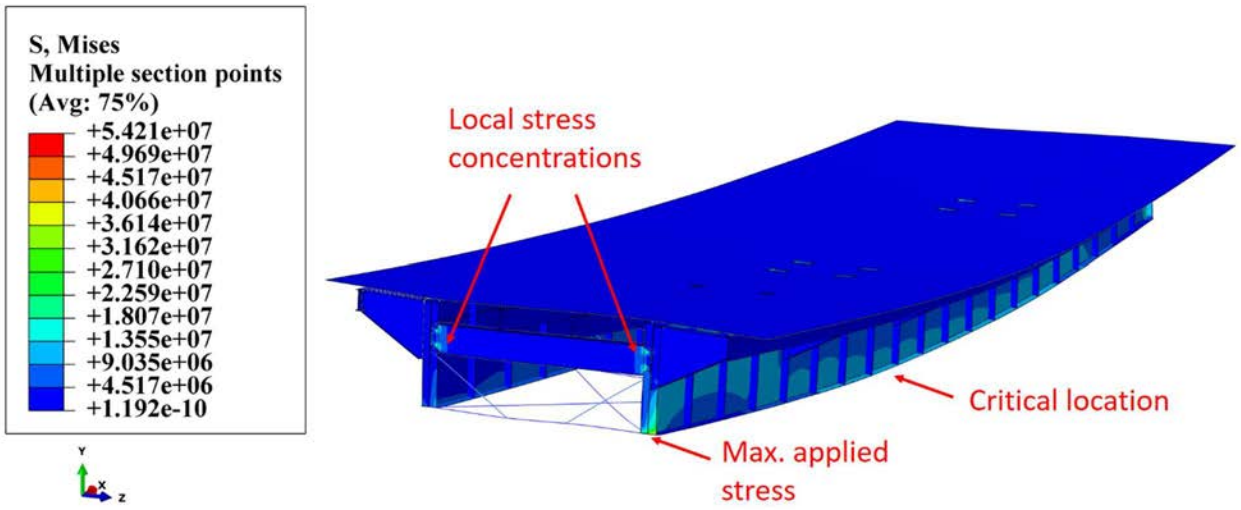

Figure 25 Uncracked bridge - Von Mises stresses (amplified by 300)

Figure 27 shows the global system deformation of the cracked bridge. Comparing those deformations with the deformations of the uncracked bridge, confirms the expectations that the existence of a crack results in an amplification of the system's deformation. For this specific example with a crack length of 2.27m, the vertical displacement in the negative y-direction increased from 0.0035m to 0.007m (Figure 24 and Figure 26), which represents an increase of 50%. Also the distortion about the x – axis and the associated out-of-plane motion increased noticeably. However, the displacement is significantly smaller than the deformation measured after the failure of the US-52 bridge in St. Paul, Minnesota which was 0.17m.

Figure 27 shows the von Mises stress distribution for the bridge with a crack of the length of 2.27m. The crack results in high local stresses at the crack tip of 147.6MPa. All other parts of the bridge are visualized almost consistently blue since their stresses are very low compared to the high stresses at the crack tip.

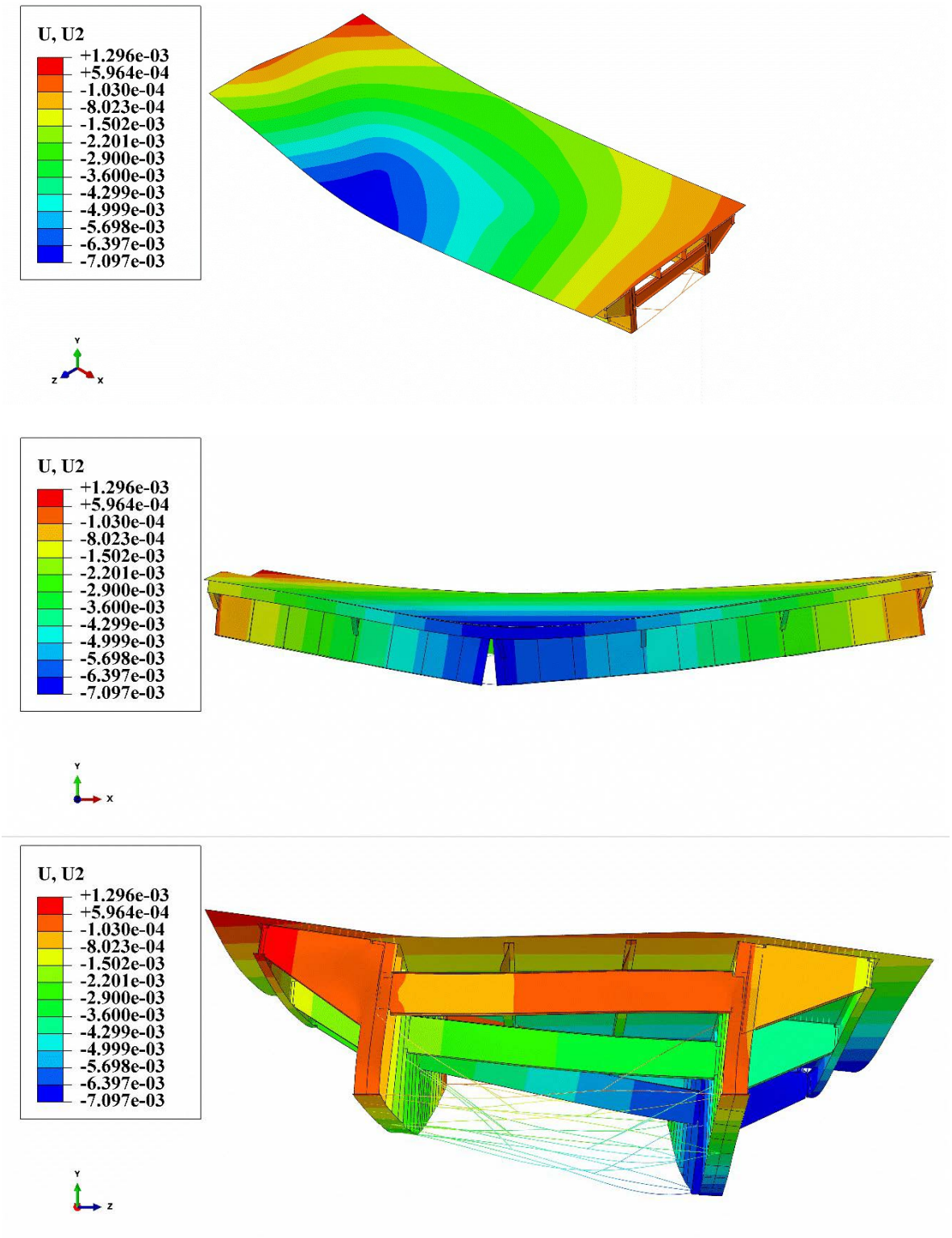

Figure 26 Global deformation in vertical direction of cracked bridge (amplified by 300)

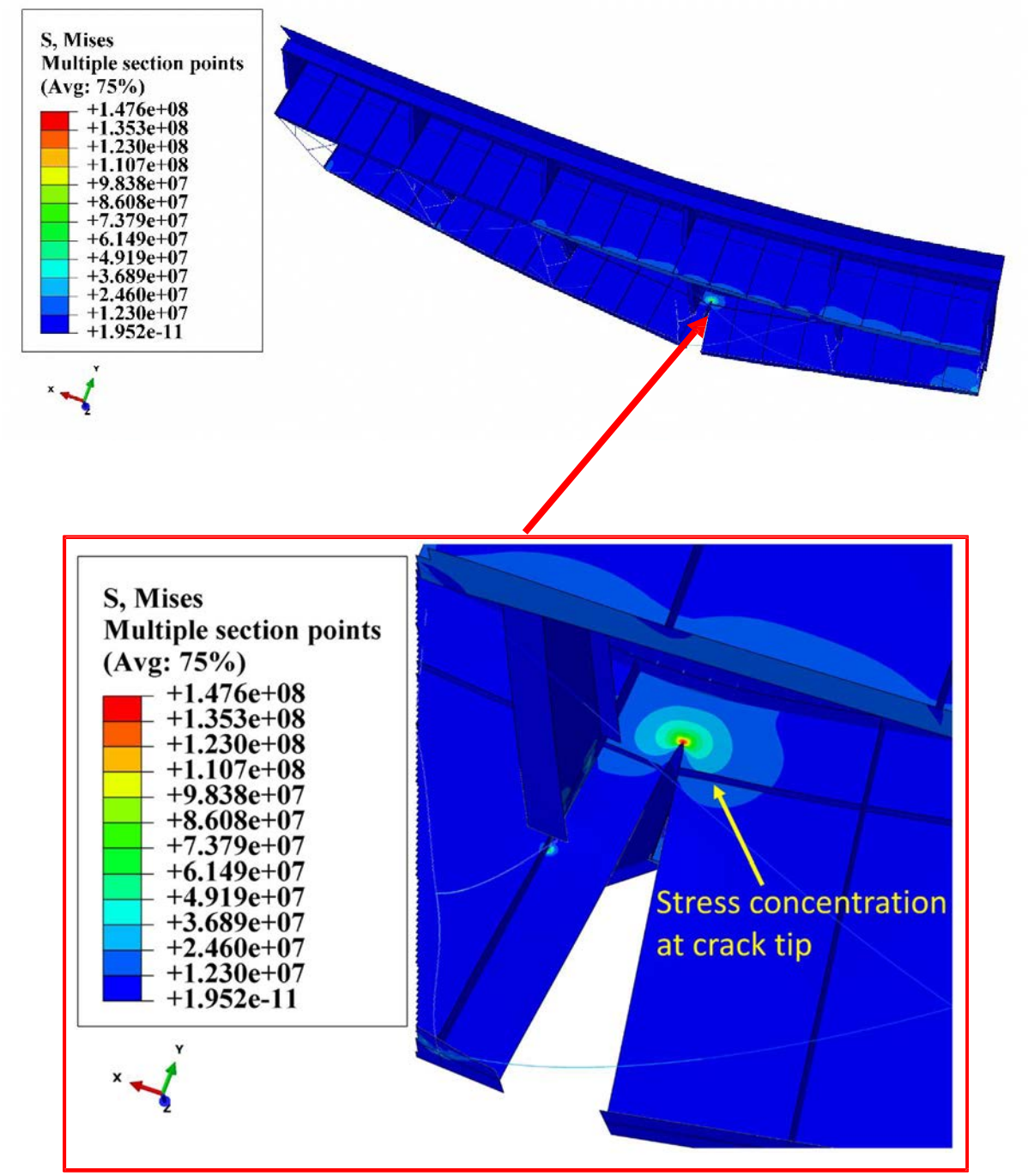

Figure 27 Von Mises Stresses in the Cracked Girder showing Localized Stress Concentration around the Crack Tip

5.2 Statistical evaluation of stress σ_{11}

For the calculation of the stresses in σ_{11} direction the numerical model of the bridge without crack was used. The stresses were evaluated at the bottom flange of one of the girders at which in subsequent simulations the crack was located. The direction 11 is along the girder and the values for σ_{11} are tensile stresses due to the bending moment caused by the truck load. During the Monte Carlo simulation, the load amplification factor and the young's modulus were treated as random variables. Both input variables were described by Gaussian normal distributions with means of 1.05Fy and 1.13, respectively. The coefficient of variation was 0.1 for both distributions.

The Monte Carlo simulation was conducted 3 times with 30, 50 and 75 iterations. The simulation results are shown in the scatter plot in Figure 28. The stresses vary between a maximum value of 31Mpa and a minimum value of 2.5 MPa. The maximum as well as the minimum value occurs for the simulation with 50 iterations. Figure 28 verifies the necessity of the probabilistic analysis. It appears that minor variations in the loading or the material properties can lead to a non-negligible increase of the stresses which can be crucial for determining the fatigue life.

The detail examined in this study belongs to fatigue category E' for which the fatigue threshold is 18MPa (AASHTO, 2012). That means if the stress at the location examined, exceeds 18MPa a crack initiates. As it can be seen in Figure 28 the mean stresses are about 17MPa therefore only in certain cases a crack will initiate. The probabilities that a crack initiates are listed in Table 4. This results show how important it is to consider all uncertainties in the determination of fatigue life. If only one analysis with deterministic values for the load and the material properties is conducted the chance for predicting crack initiation is about 45%, which is a high risk to take for the bridge owner.

The results for σ_{11} are also used to determine the minimum number of iterations needed for accurate results in the probabilistic analysis. Therefore, the Monte Carlo simulation is conducted three times with 30, 50 and 70 iterations. For each of the simulation the mean of the tensile stresses is computed and compared. Table 6 lists the mean stresses and the percentage errors for the analyses. Assuming that the results are correct for 75 iterations, it can be seen that the accuracy decreases for lower number of iterations. Although a percentage error of 1.73 is still very small, the number of iterations for all further Monte Carlo simulations was chosen to be 50.

Table 6 Results of statistical stress evaluation

Number of iterations	Mean stress σ_{11}, MPa	Percentage error	Probability of crack initiation
75	17.12	-	45%
50	17.19	0.41	46%
30	17.42	1.73	47%

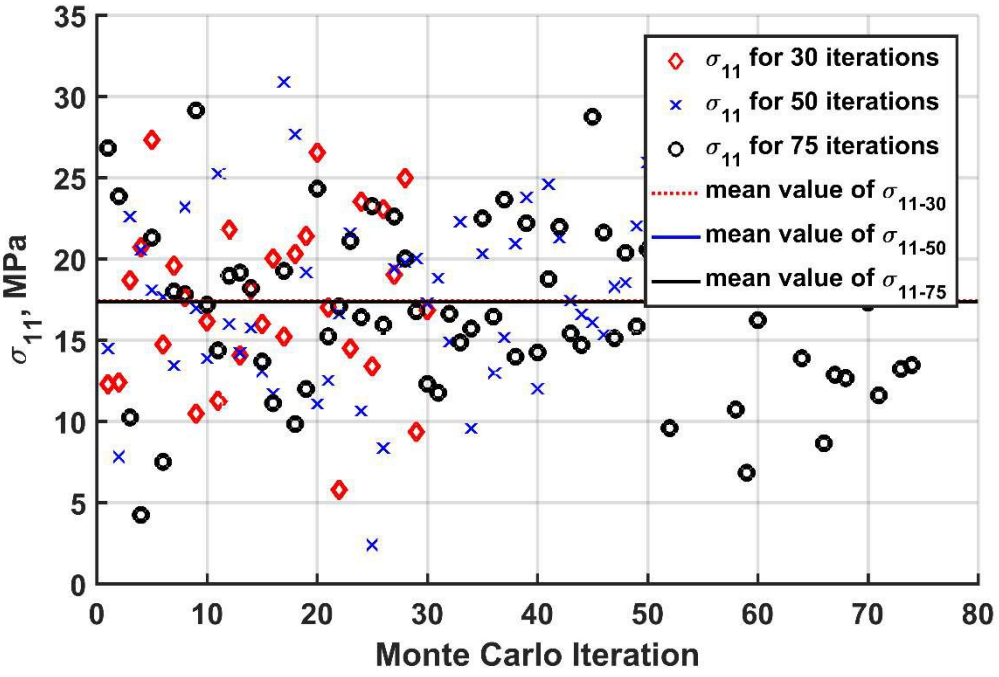

Figure 28 Scatter plot of tensile stresses σ_{11} at bottom flange of girder

5.3 Statistical evaluation of the stress intensity factor

The stress intensity factors are calculated using the finite element software ABAQUS. A crack is inserted and propagated through the flange and the web of the girder in increments of 0.08m until full-depth fracture. For each crack length 50 stress intensity factors are generated. In the Monte Carlo simulation, the load and the Young's modulus are treated as random variables with Gaussian normal distribution. The use of LEFM was proven to appropriate since the stresses measured in the region near the crack tip are below the material's yield strength of 250MPa for all simulations. For example, a crack length of 2.27m resulted in stresses near the crack tip of 147.6MPa (Figure 27).

Furthermore, the stress intensity factors are evaluated for the model including residual stresses. The residual stresses with a magnitude of 250MPa, which is equal to the yield strength of the material, are applied in the tension zone surrounding the welds. For this purpose Faulkner's model (1975) is utilized to compute the width of the tension zone which is equal to $t_{plate} * \eta$, where η equals 4. During the finite element analysis, a compression zone is calculated to balance the tensile stresses and to satisfy equilibrium. A schematic sketch of the residual stresses along the girder is shown in Figure 29. Previous research has shown that this compression zone can slow down or even stop crack growth due to the stresses acting in the opposite direction (H. Mahmoud & Riveros, 2014). Therefore, an effective stress intensity factor ΔK_{eff} is used to assure that only the part of the stress intensity factor that contributes to crack growth is considered when computing the remaining fatigue life. ΔK_{eff} is computed by superposition of K_{min}, K_{max} and K_{res}.

K_{res} is evaluated in the compression zones on the bottom flange and the web, and where the longitudinal stiffener is welded to the girder (Figure 29). The resultant K values from the ABAQUS simulation are exclusively positive and it is found that the compression zones do not affect the

crack propagation rate (Table 7). Due to this, ΔK_{eff} is equal to K_{max} resulting from the applied load and the residual stresses are neglected.

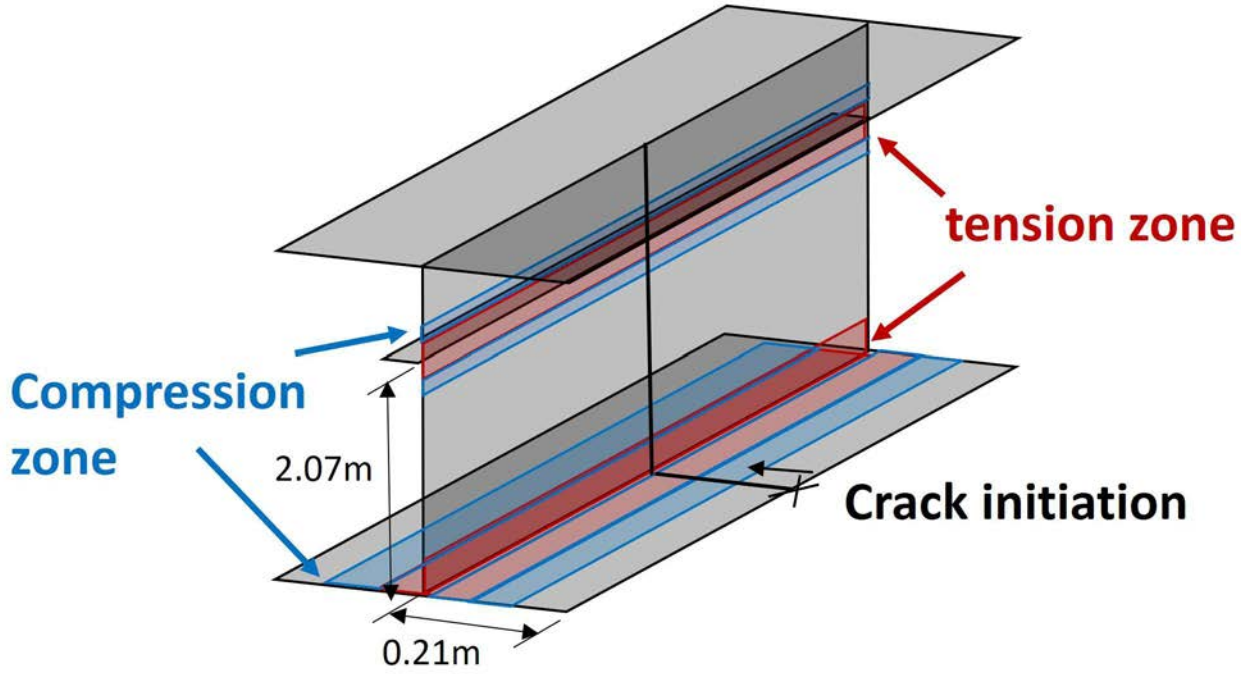

Figure 29 Schematic sketch of residual stresses along girder

Table 7 Stress intensity factors in compression zones

Crack length, m	K, Mpa(m)$^{1/2}$
0.16	22.8
0.31	89.8
2.00	24.3
2.20	53.0

Figure 30 shows the stress intensity factors and its variation with respect to the crack length. The values for K are clearly varying due to the randomness in the input data. For clarity, the plot shows the root mean square of all 50 stress intensity factor curves and its deviations. It can be seen

that the stress intensity values increase consistently during the first crack intervals. However, after a crack length of 0.47m it stagnates and then only increases with a small slope. That means the influence of the crack length on the stress intensity factor decreases with increasing crack length. This is due to the shift in the neutral axis of the cross section as the crack propagates and load shedding which causes the stresses to redistribute around the cracked region. At a crack length of 1.43m the stress intensity factor reaches its maximum value. The change in the slope occurs due to the transition from the tension to the compression zone. The compression works against the crack opening and therefore slows down the crack propagation rate and results in a decrease of K. The K values decrease until it reaches the longitudinal stiffener at 2.09m which leads to a short increase of K. Afterwards the value decreases until full depth fracture at 2.5m.

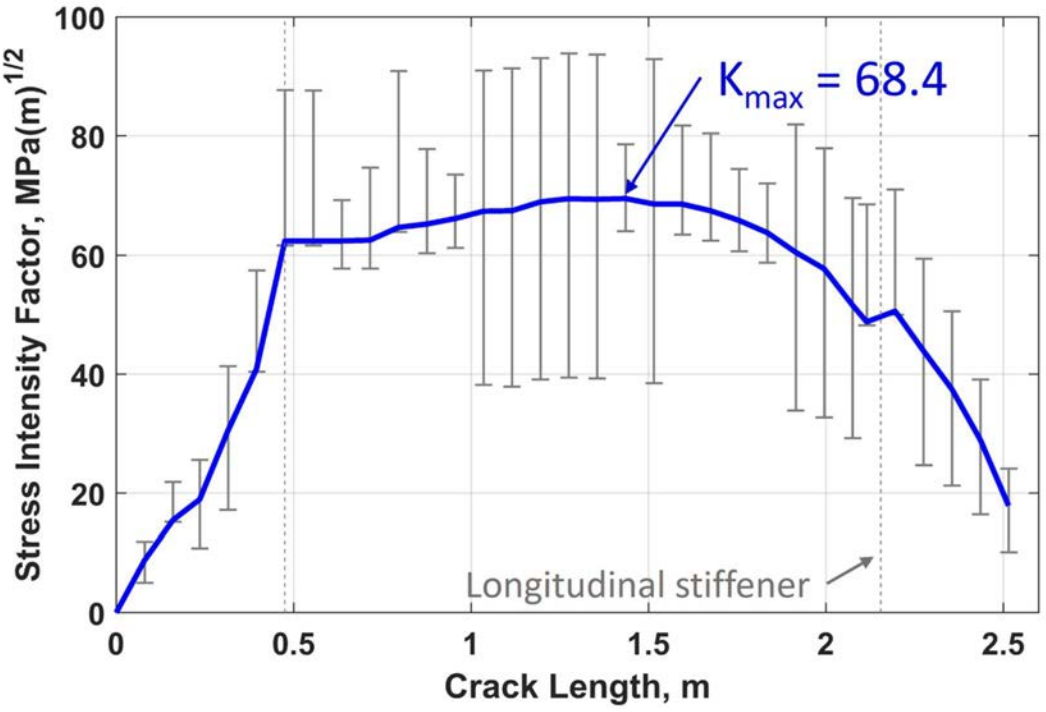

Figure 30 Root mean square of stress intensity factors and its variation

For further processing of the data each of the 50 K – curves were smoothened by a second-degree polynomial. Figure 31 shows the fitting of the highly varying stress intensity curve from the ABAQUS simulation with a second-degree polynomial.

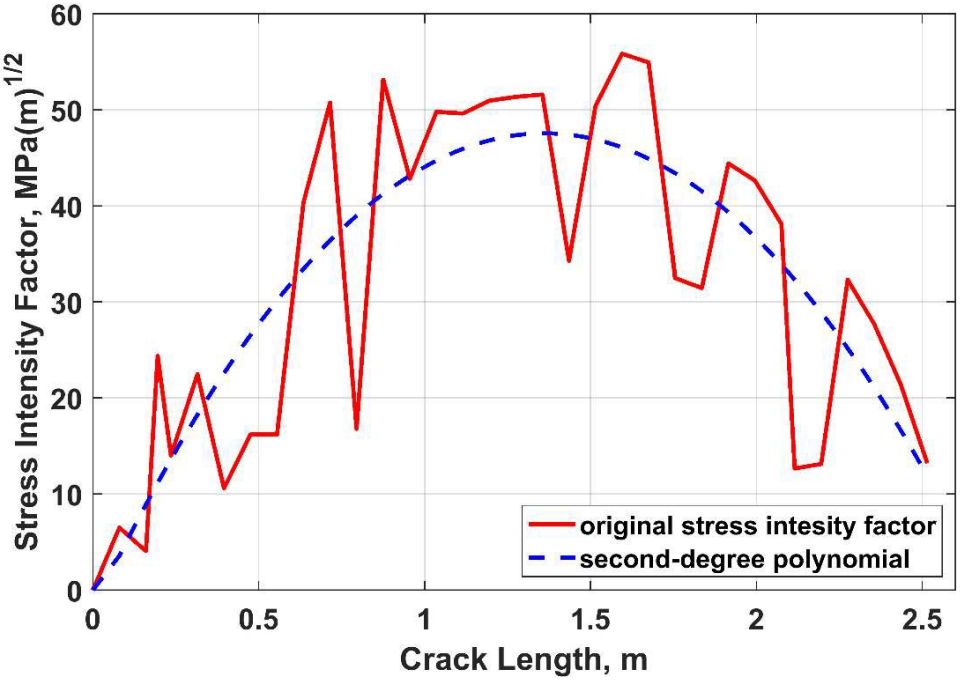

Figure 31 Original stress intensity factor curve and fitting curve using a second-degree polynomial

5.4 Statistical evaluation of the remaining fatigue life

For the statistical evaluation of the remaining fatigue life the results from the previous analysis of the stress intensity factors where the load and the material properties are treated as random variables are used. The Paris Law (Paris & Erdogan, 1963) was utilized to calculate the number of cycles until failure. Failure occurs when the maximum stress intensity K exceeds K_{IC}, which is taken as 45MPa$(m)^{1/2}$, 65MPa$(m)^{1/2}$, 75MPa$(m)^{1/2}$ and 95MPa$(m)^{1/2}$. Since the material toughness K_{IC} only indicates the point at which a crack starts to propagate in an unstable manner but does not provide information about the possibility of the crack getting arrested due to changing

condition such as the transition into a compression zone, K is also compared to the crack arrest toughness K_a. If K exceeds K_a the crack velocity and the crack's momentum are sufficient enough so that the crack travels through the girder without getting arrested.

The crack propagation parameters C and m in the Paris Law were assigned a Gaussian normal distribution with a mean of 3 for m and a mean of $9.0*10^{-12}$ for C, respectively. The COV are taken as 3.0 and $0.25*10^{-12}$ as recommended by British Standards (1997). A plot of the crack length versus the number of cycles is displayed in Figure 32. It is apparent that the statistical variation of C and m has immense influence on the crack growth behavior and therefore on the crack propagation rate. It is noticeable that there is an enormous scatter in the number of cycles needed to propagate the crack through the whole girder. This shows the need for a statistical evaluation to enhance the understanding for the scatter in fatigue data. Figure 33 through Figure 35 show the crack length at failure for material toughness of $45MPa(m)^{1/2}$, $65MPa(m)^{1/2}$.and $75MPa(m)^{1/2}$. The crack length at failure is not plotted for $95MPa(m)^{1/2}$ since K is always smaller than this value. The plots show that for higher material toughness the crack length that the girder can tolerate before the crack starts to propagate in an unstable manner is significantly higher. For a material toughness of $75MPa(m)^{1/2}$, the crack does not exceed the crack arrest toughness in 74% of the cases.

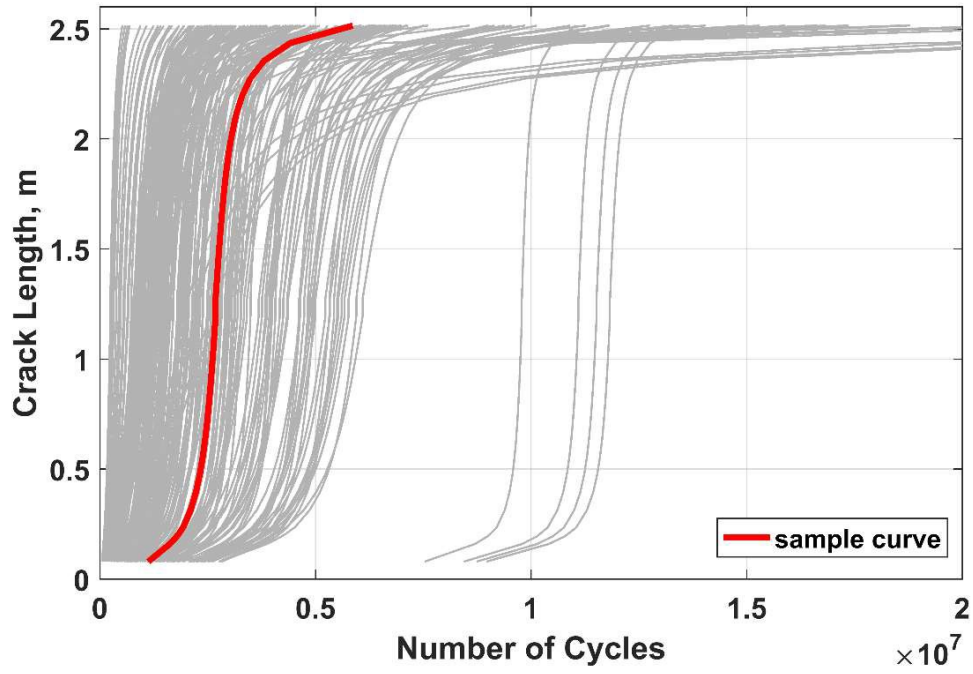

Figure 32 Crack length versus number of cycles

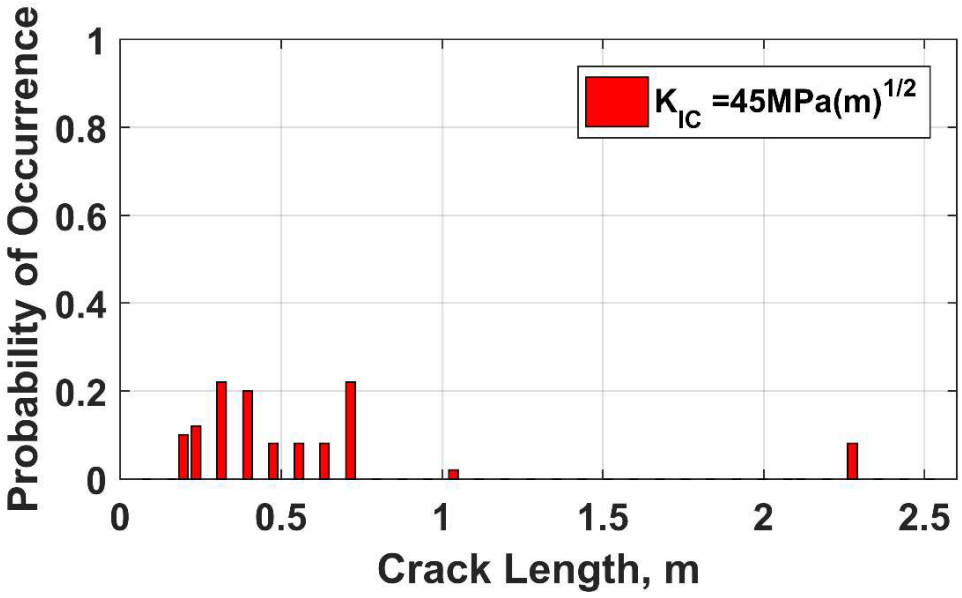

Figure 33 Probability of occurrence for K_{IC} = 45MPa(m)1/2

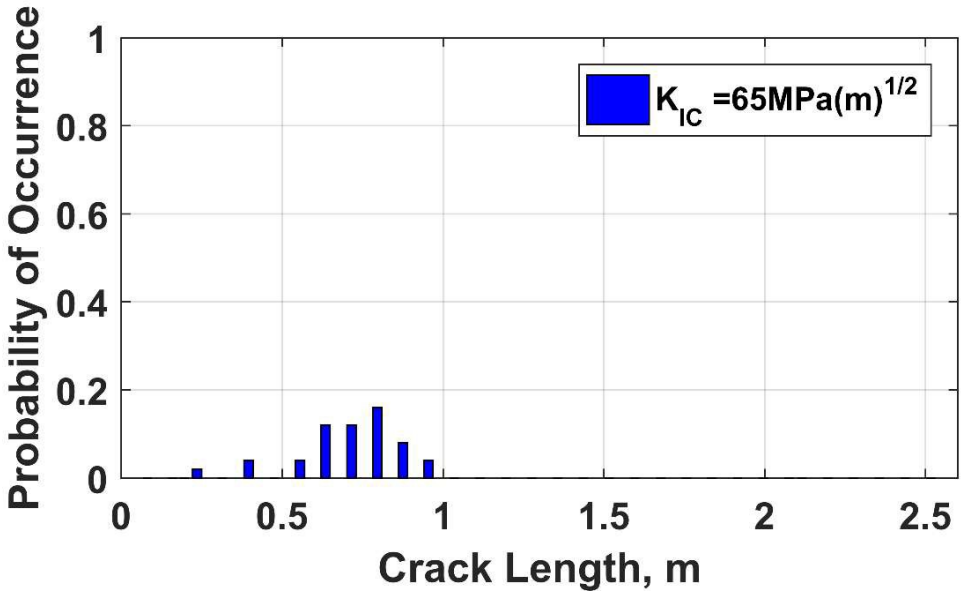

Figure 34 Probability of occurrence for K_{IC} = 65MPa(m)1/2

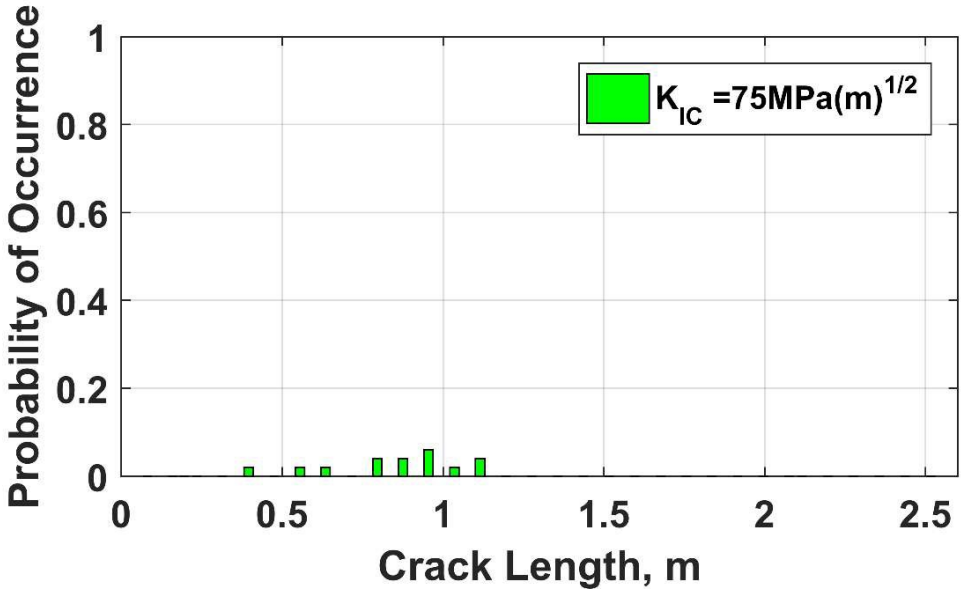

Figure 35 Probability of occurrence for K_{IC} = 75MPa(m)1/2

The probability of failure and the corresponding reliability index are calculated for different inspection intervals. Failure is defined to occur when the number of cycles per inspection interval exceeds the number of cycles to failure. For the evaluation of this study the inspection intervals are chosen to be in a maximum interval of 7 million cycles. The probability of failure and

the corresponding reliability index are calculated for critical fracture toughness values of 45MPa(m)$^{1/2}$ 65MPa(m)$^{1/2}$, 75MPa(m)$^{1/2}$ and 95MPa(m)$^{1/2}$. Comparing the stress intensity factor to the material toughness K_{IC} provides the engineer with a general idea about the structure's susceptibility to failure. However, it does not consider the possibility that the crack might be arrested when entering the compression zone. To take crack arrest into account it is necessary to compare K to the crack arrest toughness K_a, since this value considers dynamic effects such as the crack propagation velocity. Therefore, the probability of failure and the corresponding reliability index are also computed for crack arrest toughness of 55MPa(m)$^{1/2}$, 60MPa(m)$^{1/2}$ and 70MPa(m)$^{1/2}$. These values are the results of research conducted by Ripling and Crosley (1982). The values are chosen in accordance with the temperature zones defined by AASHTO (2012). The temperatures and the corresponding crack arrest toughnesses are listed in Table 8.

Table 8 Temperature zones and corresponding crack arrest toughnesses K_a

Temperature zone	Lowest anticipated service temperature	K_a
1	-18°C and above	70 at -18°C
2	-18 to -34°C	60 at -35°C
3	-35 to -51 °C	55 at -51°C

The probability of failure curve and the corresponding reliability index are shown in Figure 36 through Figure 39. The plots confirm the assumption that for a higher material toughness the probability of failure is smaller. Furthermore, it can be seen that for a lower number of cycles per inspection interval the probability of failure is smaller. This is reasonable since if a structure is inspected more frequently the chance that the structure fails between two inspections is smaller. However, a higher reliability index is associated with more safety and therefore the reliability

index with respect to the number of cycles per inspection interval shows an inverse correlation. With increasing inspection intervals, the chances that cracks remain undetected increases and thus the probability of failure increases and the reliability index decreases.

The results also show the influence of higher material strength on the structure's ability to resist cracks. When the material toughness is increased from 45MPa$(m)^{1/2}$ to 65MPa$(m)^{1/2}$, 75MPa$(m)^{1/2}$ and 90MPa$(m)^{1/2}$ a tremendous decrease in the probability of failure occurs. For a fracture toughness of 45MPa$(m)^{1/2}$ a probability of failure of 20% occurs for an inspection interval of 700,000 cycles. For the same probability of failure the inspection interval can be increased to 3,4 million cycles for a material toughness of 75MPa$(m)^{1/2}$.

The maximum reliability index that can be achieved is 3.8 for material toughness of 65MPa$(m)^{1/2}$ and 95MPa$(m)^{1/2}$. For all material toughness the reliability index steadily decreases with increasing inspection interval until it reaches its final value. The tougher the material the faster it approaches its final value. These results show that by only increasing the fracture toughness slightly a tremendous increase in the fatigue life can be achieved.

The probability of failure and the corresponding reliability index when considering crack arrest are shown in Figure 38 and Figure 39. The probability that a crack zips through the girder without being arrested is with a minimum of 46% at a temperature of -18^{o}C very high. However, K_a increases with increasing temperature that mean in an area with higher average temperature the probability of failure decreases. The reliability index is computed for K_a values of 55MPa$(m)^{1/2}$, 60MPa$(m)^{1/2}$ and 70MPa$(m)^{1/2}$. The maximum achievable reliability index is 2.5 for an inspection interval of 150,000 cycles for K_a =60MPa$(m)^{1/2}$. It is important to point out that the probability of failures or reliability indices reflect a crack growing through the full depth of the girder not a bridge collapse. Figure 38 and figure 39 provide an illustration on how inspection intervals can be

determined for a desired probability of failure for a given fracture toughness. In other words a bridge owner can conduct a similar analysis on the bridge in question then extract steel samples from the actual bridge to determine the fracture toughness the construct a similar plot to show the probability of failure versus inspection interval so that a proper inspection cycle can be determined.

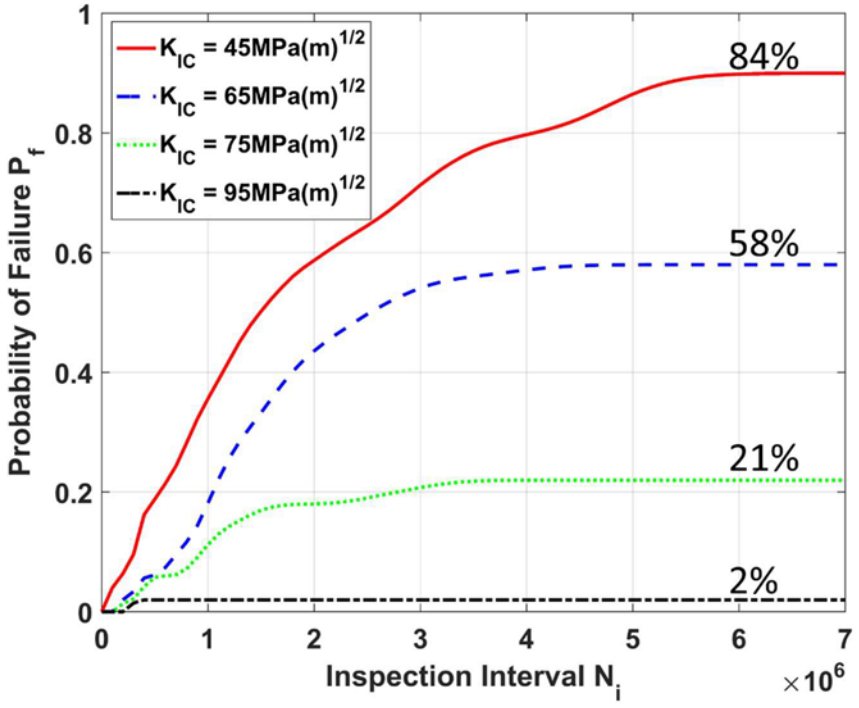

Figure 36 Probability of failure versus inspection interval Ni without accounting for crack arrest

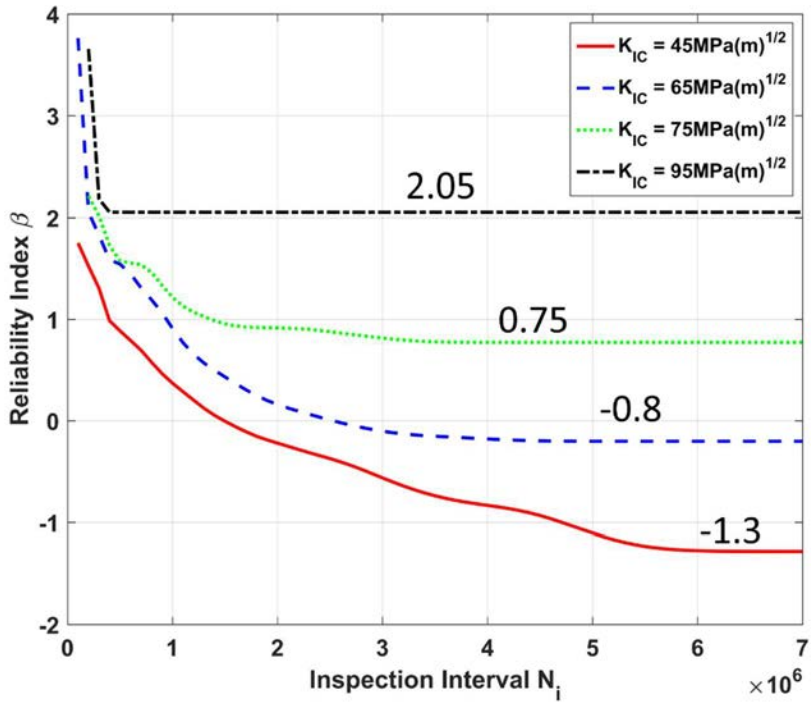

Figure 37 Reliability index versus inspection interval Ni without accounting for crack arrest

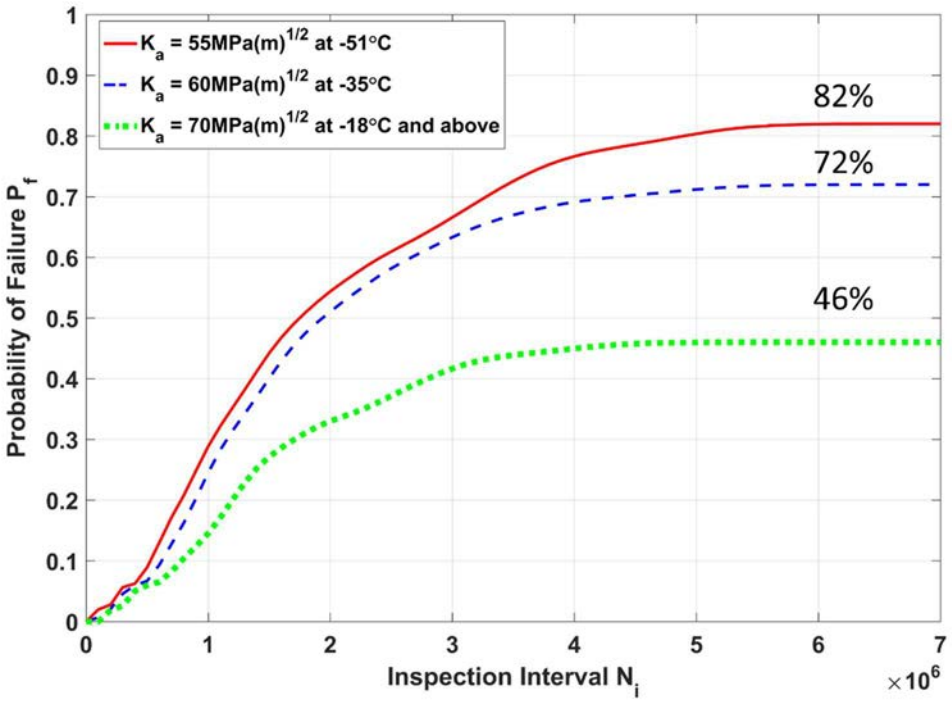

Figure 38 Probability of failure versus inspection interval Ni when accounting for crack arrest

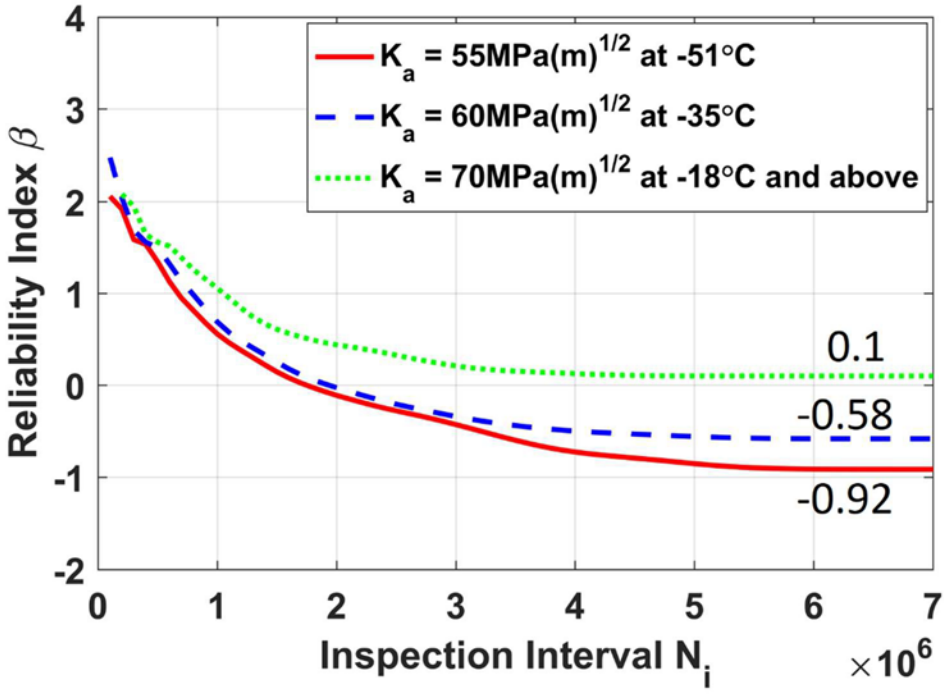

Figure 39 Reliability index versus inspection interval Ni when accounting for crack arrest

5.5 Bridge Redundancy and Potential for Collapse

As discussed in previous chapters, several bridge failures with full depth fracture of a main supporting member, classified as fracture critical, occurred without resulting in collapse of the complete structure. This identifies that the classification of bridges in the category fracture critical is not sufficient to predict collapse. To certainly identify collapse, redundancy needs to be considered and assessed. At this point, there is no consistent and generally applicable definition of redundancy. However, effort has been made to come up with a formulation describing redundancy for multiple bridge types. For example, Frangopol & Curley (1987), developed a redundant factor R using the overall collapse load of the damaged structure and of the intact structure. Another description of redundancy was proposed by Furuta, Shinozukam, & Yao (1985). They described redundancy as a function of member properties, reduction in the members' geometry and a

constant representing the members' original geometrical properties. In this thesis the redundancy of the bridge is investigated by comparing the equivalent plastic strain ε_{pl} to the failure strain of steel ε_f for various bridge elements for several crack lengths. Utilizing the equivalent plastic strain, allows for the strain to be defined for a completely arbitrary stress states caused by arbitrary deformations. Setting this value in relationship to the failure strain gives a criterion that can be used to define failure

$$\frac{}{} < 1 \qquad \text{no failure} \qquad (5.1)$$

$$\frac{}{} \geq 1 \qquad \text{failure} \qquad (5.2)$$

The equivalent plastic strain is computed for the maximum design load as defined in AASHTO (2012) (Chapter 3). The maximum design load contains the lane load plus the truck load and the applicable amplification factors. Table 9 lists the stress intensity factors and the equivalent plastic strains for five different crack length.

Table 9 K values and equivalent plastic strain for various crack length

Crack length in m	K in Mpa$(m)^{1/2}$	ε_{pl}
0.215	56.472	3.78e-3
0.475	362.545	-
1.355	406.26	-
2.555	33.261	6.75e-3
2.77	0	1.44e-1

For a crack length of 0.215m, which is equivalent to a cracked flange, the K_{IC} value is 56.472

$Mpa(m)^{1/2}$. Assuming a K_{IC} value greater than this, means that the crack is growing in a stable manner and the stresses and strains at this condition can be evaluated. The ABAQUS simulation shows that the yield stress is only locally exceeded and the bridge only locally plastifies at the crack tip.

For a crack length of 0.475m and 1.355m the stress intensity factor K exceeds the material toughness, which means that the crack would have already started to grow in an unstable manner for a shorter crack length. Thus, this condition is not realistic and cannot be evaluated. The next crack length that results in a stress intensity factor of less than KIC is 2.555m, which is equivalent to a crack through the bottom flange, through the web all the way up to the top flange. At this point, the crack tip is in the compression zone. The compressive forces due to the girder bending slowed down the crack propagation and led to the decreased K value Table 9. The damage of the girder results in local stresses equal to the yield stress of the material at the connections of the floor beam to the girder of bay four and bay six (Figure 40). These two locations are stressed the most due to the sagging of the bridge. The load is redistributed along the system and additional moments are induced into these connection points due to the rotation of the bridge about the x-axis. Detailed views of the local plastification is shown in Figure 41 through Figure 44. An increase of the stresses above the yield strength leads to permanent deformation and plastification. The equivalent plastic strain measured for a completely cracked web is with a maximum value of 6.75e-3 at connection C3, which is much smaller than the equivalent plastic strain ε_f=0.2 and therefore the connection will not fracture

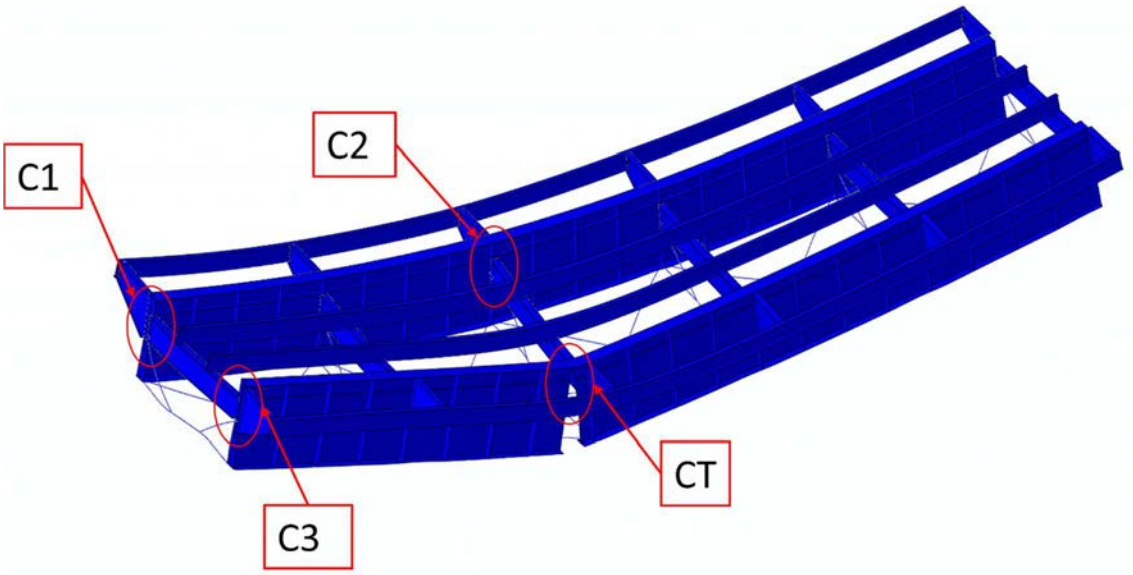

Figure 40 Bridge structure identifying locations of plastification for a crack length of 2.555m

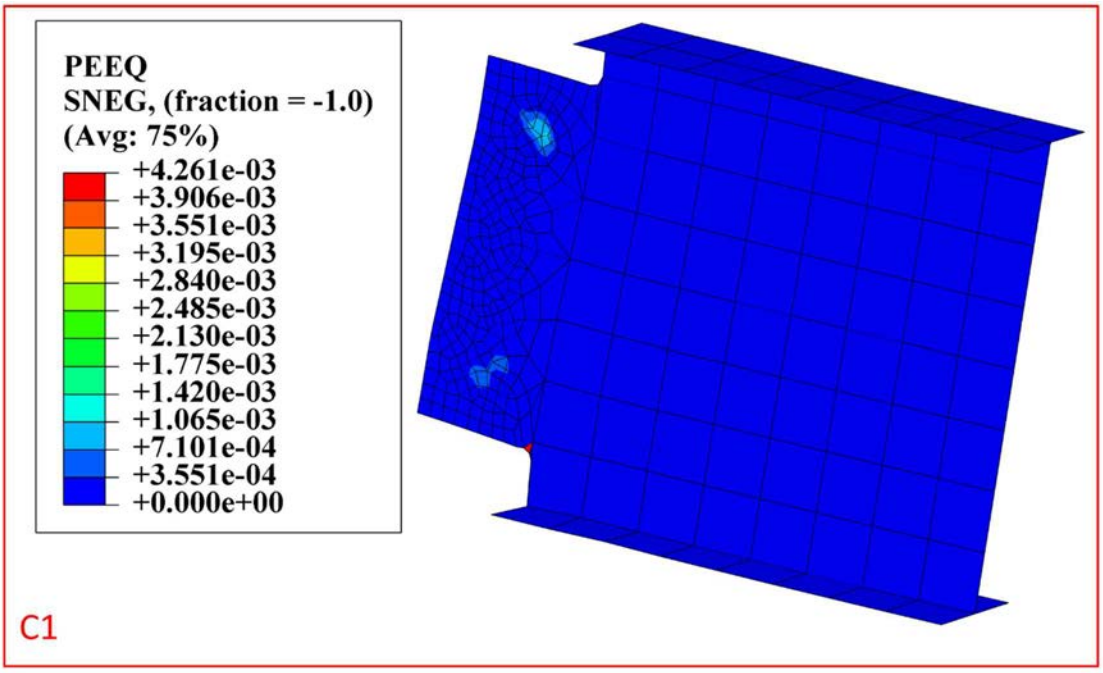

Figure 41 Plastification at connection C1 for a crack length of 2.555m

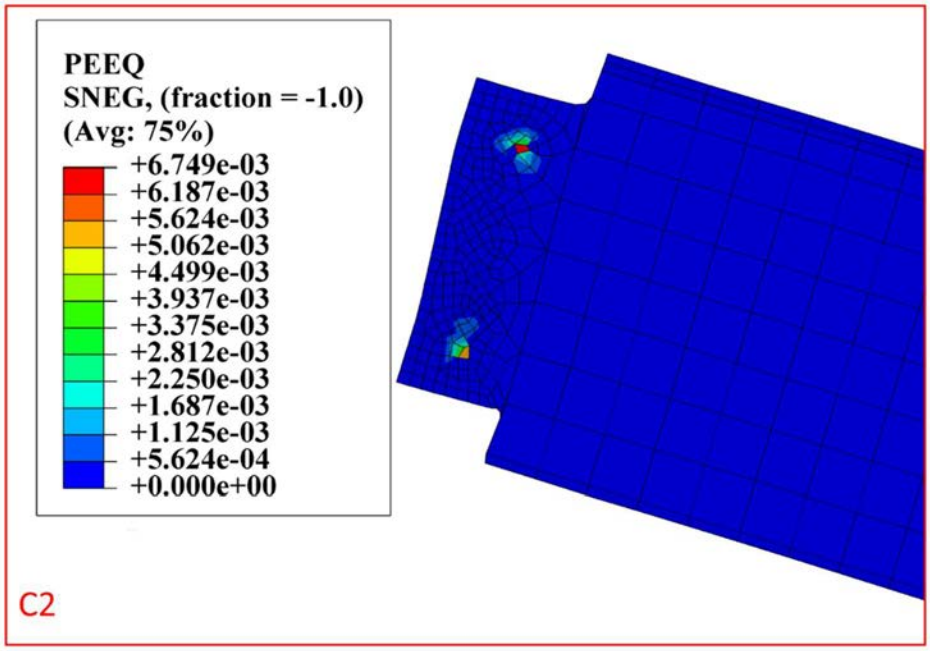

Figure 42 Plastification at connection C2 for a crack length of 2.555m

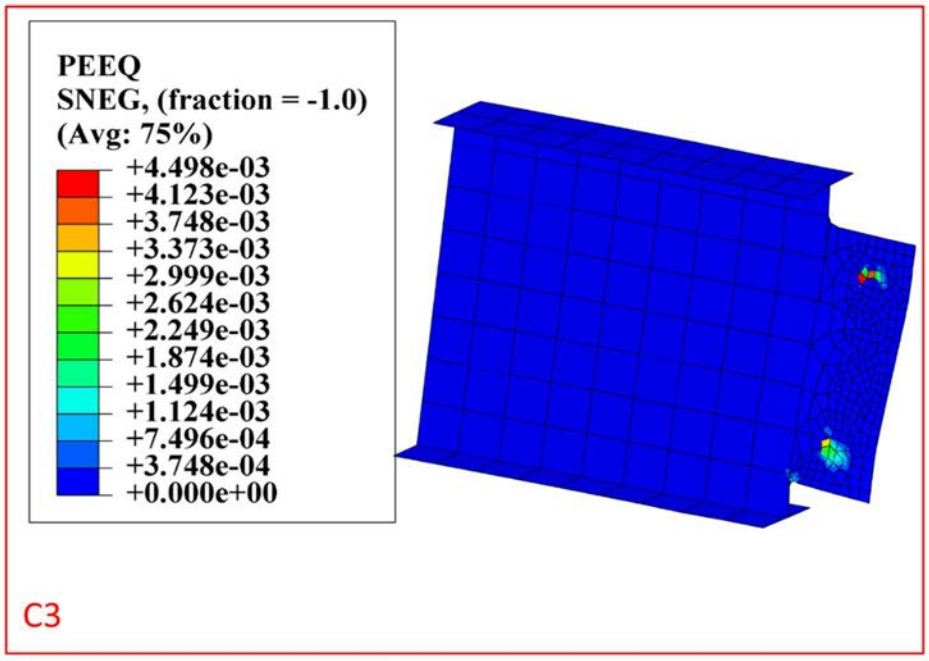

Figure 43 Plastification at connection C3 for a crack length of 2.555m

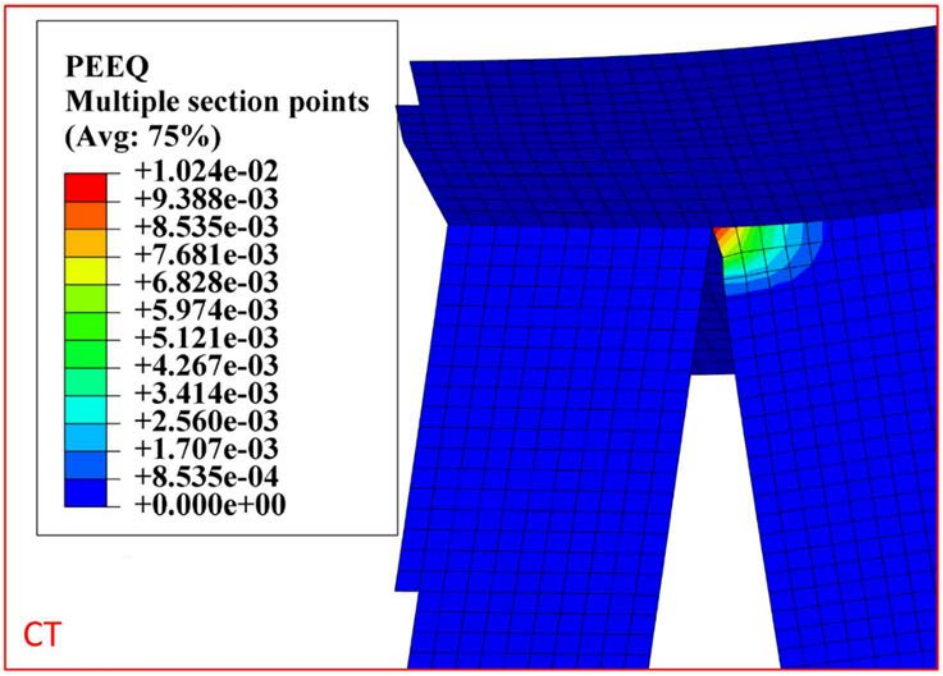

Figure 44 Plastification at the crack tip for a crack length of 2.555m

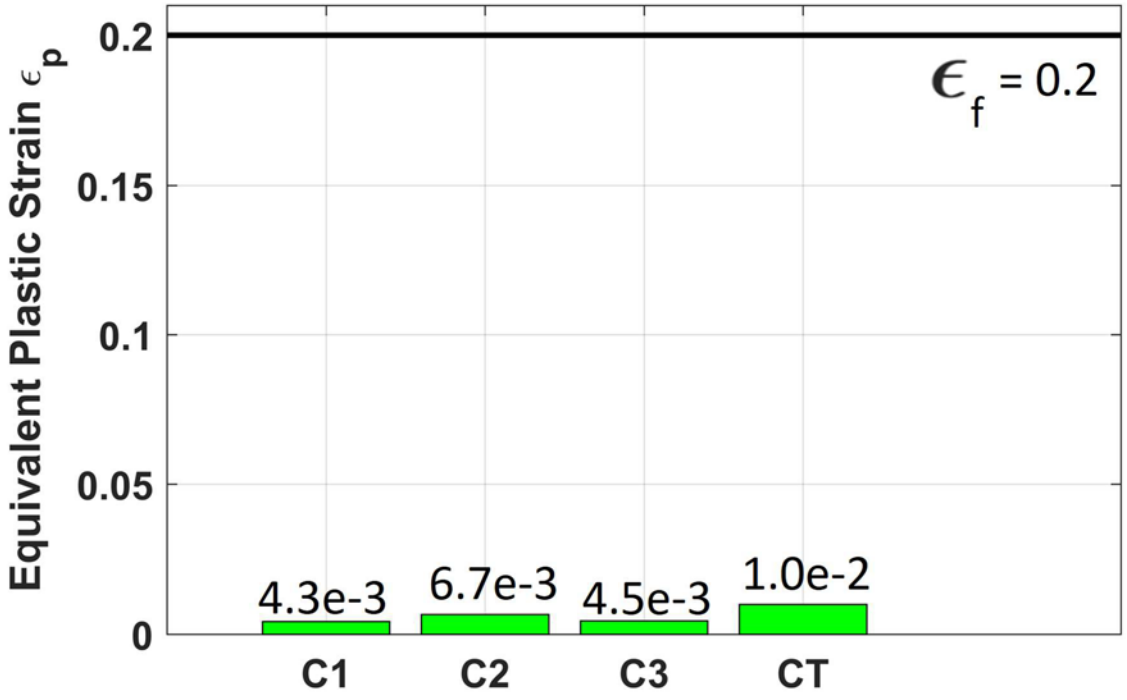

Figure 45 Equivalent plastic strain for connection C1, C2, C3 and the crack tip CT

Since the K value for a completely cracked web is smaller than K_{IC} the crack keeps growing in a stable manner until fracture. At this point the girder is separated into two pieces and the stress intensity factor is zero. The sudden fracture of the whole girder leads to a sudden increase of the forces acting on the remaining intact members. The extreme loading results in plastification at the locations identified in Figure 46. Plastification occurs mainly at the connections of the outrigger to the girder and the floor beam to the girder but also in the bracing Figure 46. Detailed views of the local plastification is shown in Figure 47 through Figure 52.

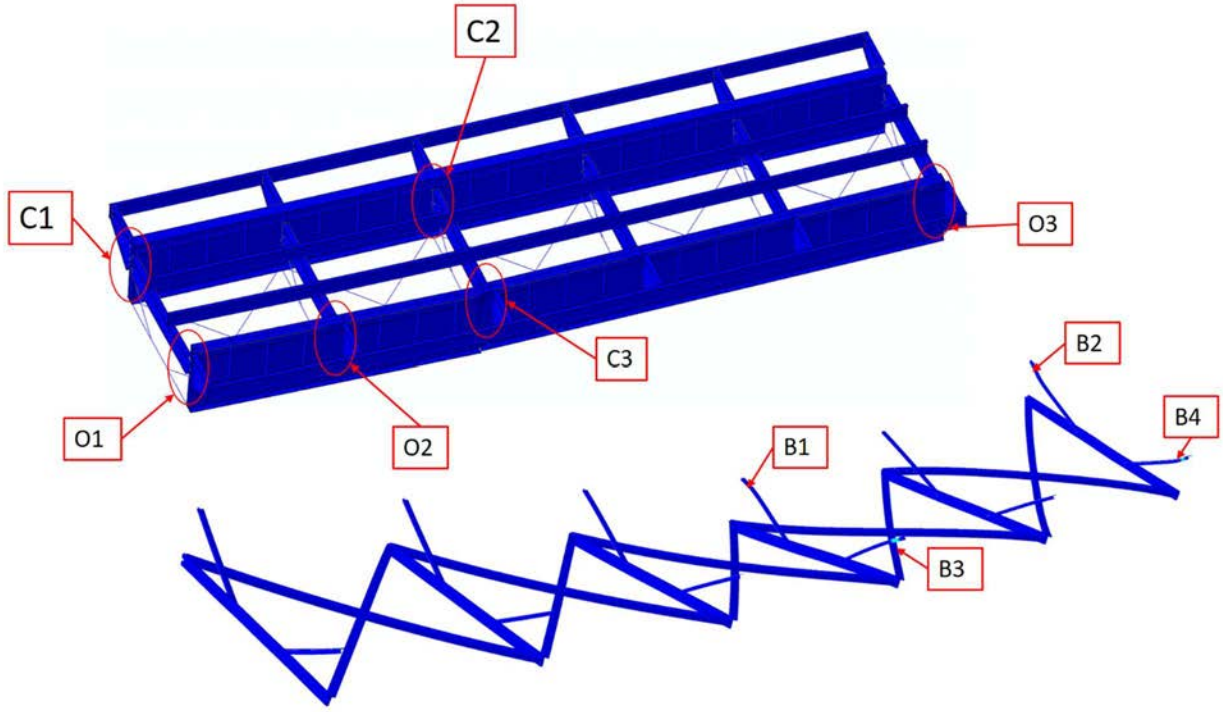

Figure 46 Bridge structure identifying locations of plastification at full depth fracture

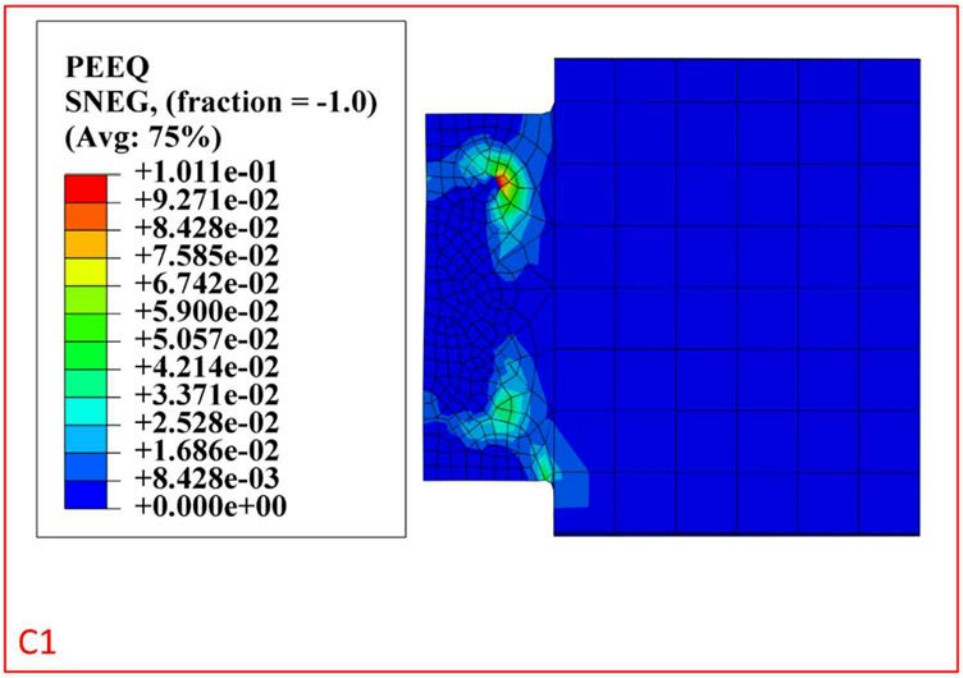

Figure 47 Plastification at connection C1 at full depth fracture

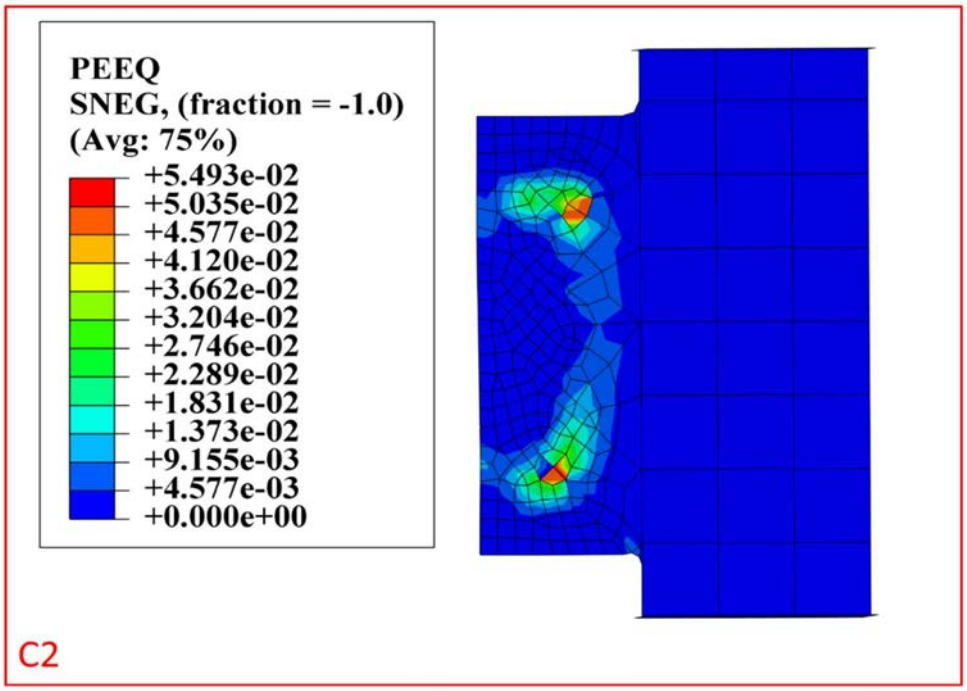

Figure 48 Plastification at connection C2 at full depth fracture

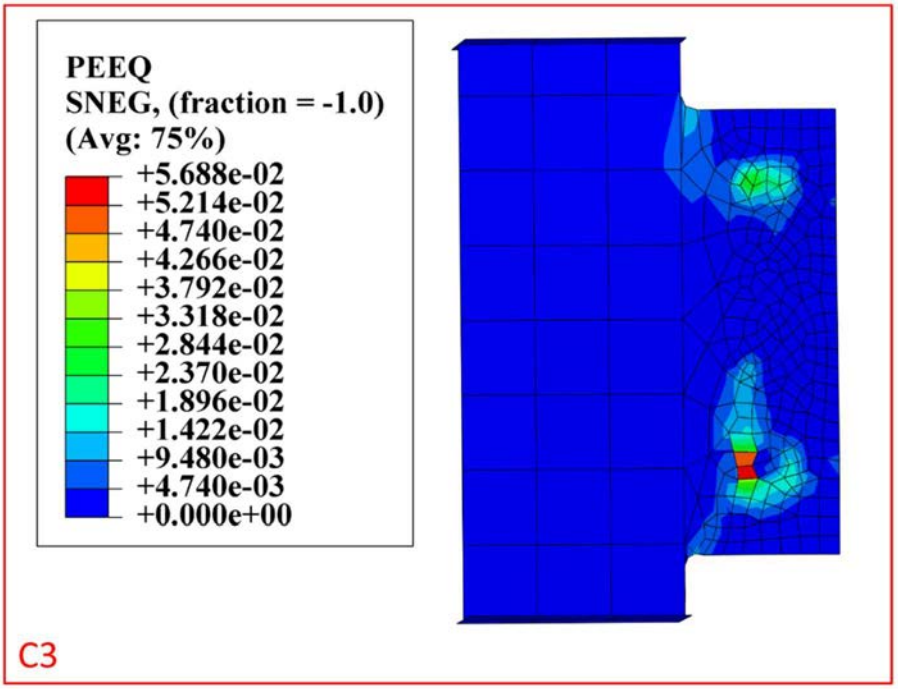

Figure 49 Plastification at connection C3 at full depth fracture

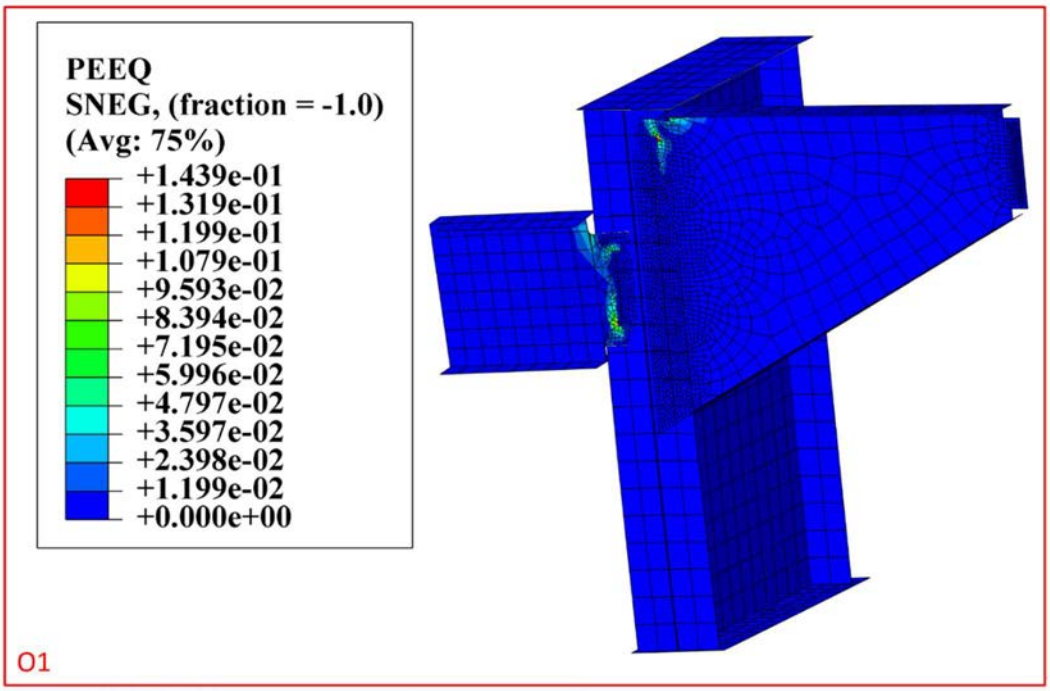

Figure 50 Plastification at connection O1 at full depth fracture

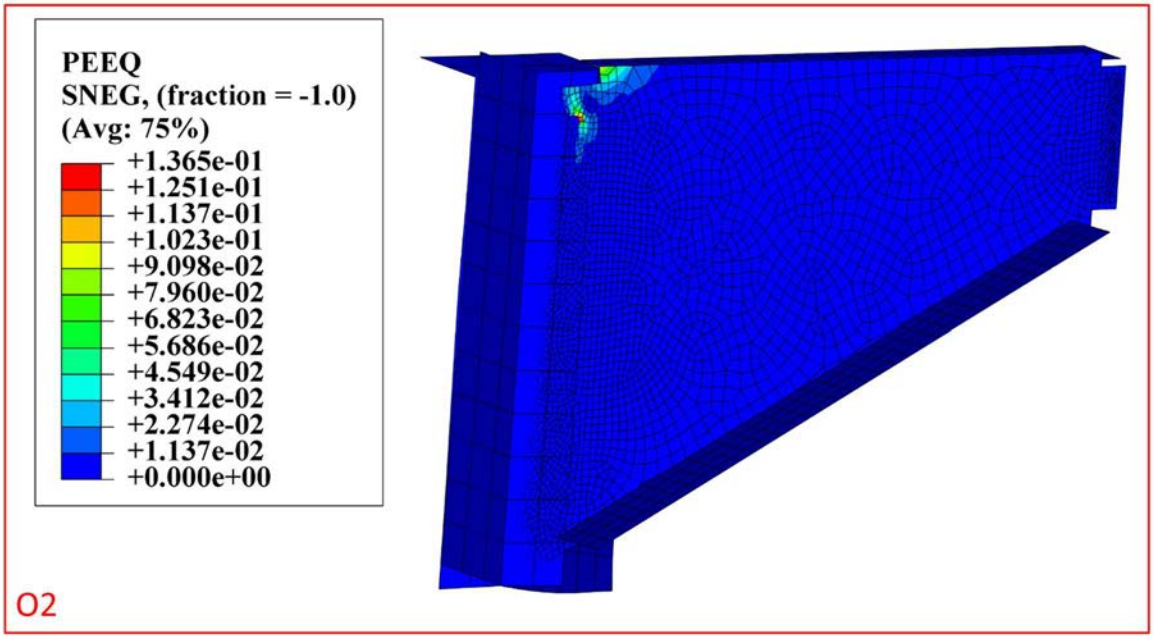

Figure 51 Plastification at connection O2 at full depth fracture

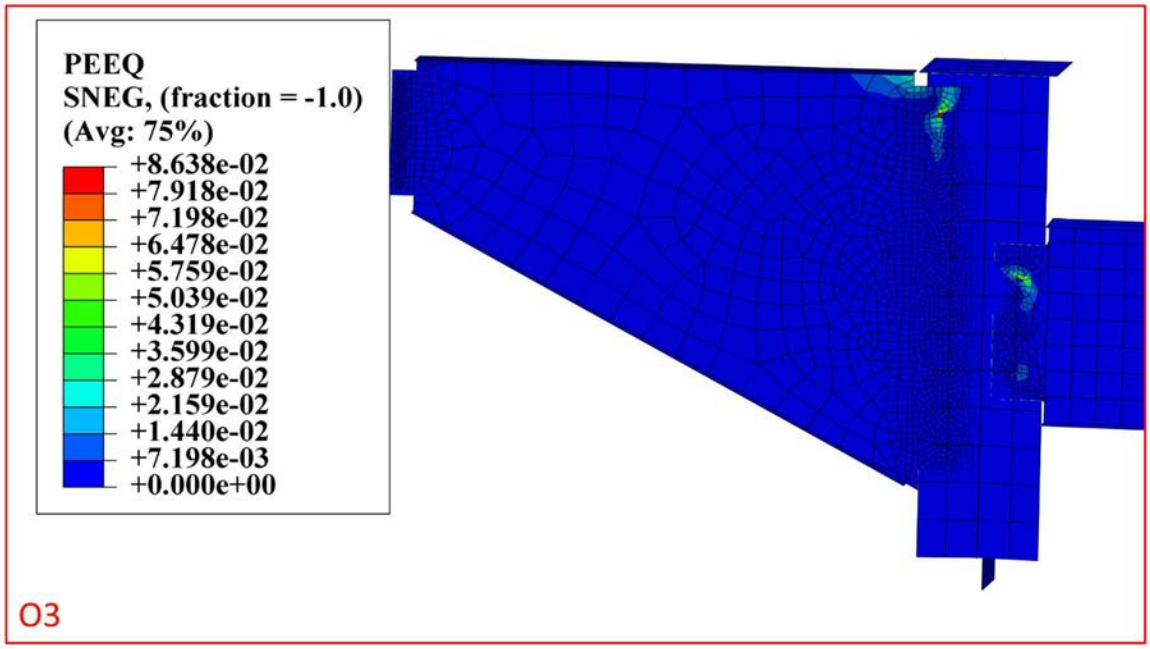

Figure 52 Plastification at connection O3 at full depth fracture

The values of the equivalent plastic strain vary between 1.5e-2 at bracing B3 and 0.144 at outrigger 1. The maximum equivalent plastic strain reached for this bridge at full depth fracture is

about 70% of the tolerable strain of the steel which means that the equivalent plastic strain does not exceed the failure strain of the steel (ε_f =0.2) for any given crack condition. Therefore, one can conclude that none of the structural members fail even though a member classified as FC is clearly yielded. This means that the bridge has significant redundancy and provides alternative load paths in the case of failure of one of the main supporting members. In other words, the classification of the Betzwood Bridge as a FCB is very conservative. The implication of such is that biannual hands on field inspection by highly qualified professional bridge inspectors is needed. This increases the inspection cost for the bridge owner. These results show that a reconsideration of the classification of bridges as FCB would be a reasonable step to decrease maintenance cost of existing bridges.

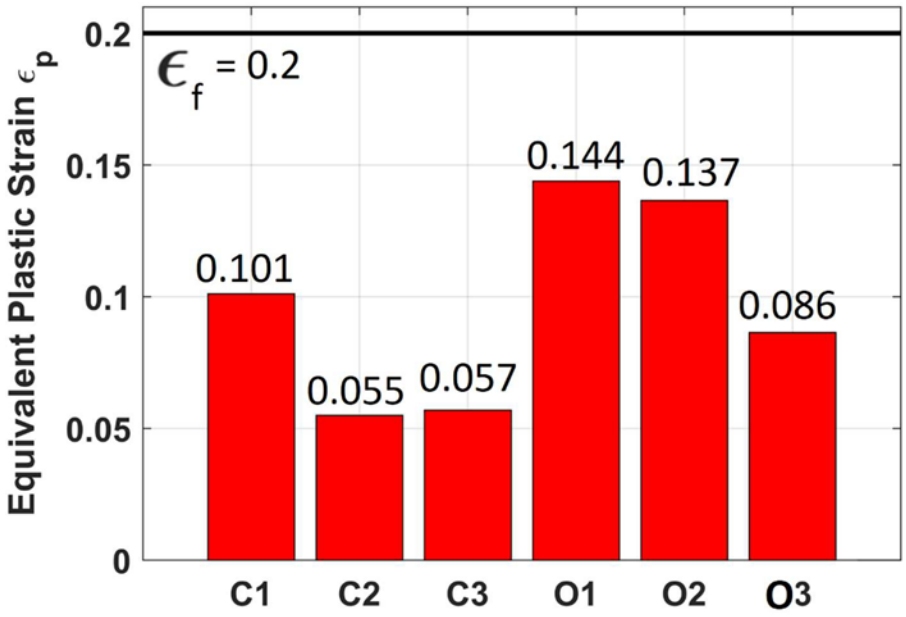

Figure 53 Equivalent plastic strain for bracing C1, C2, C3, O1, O2, O3 at full depth fracture

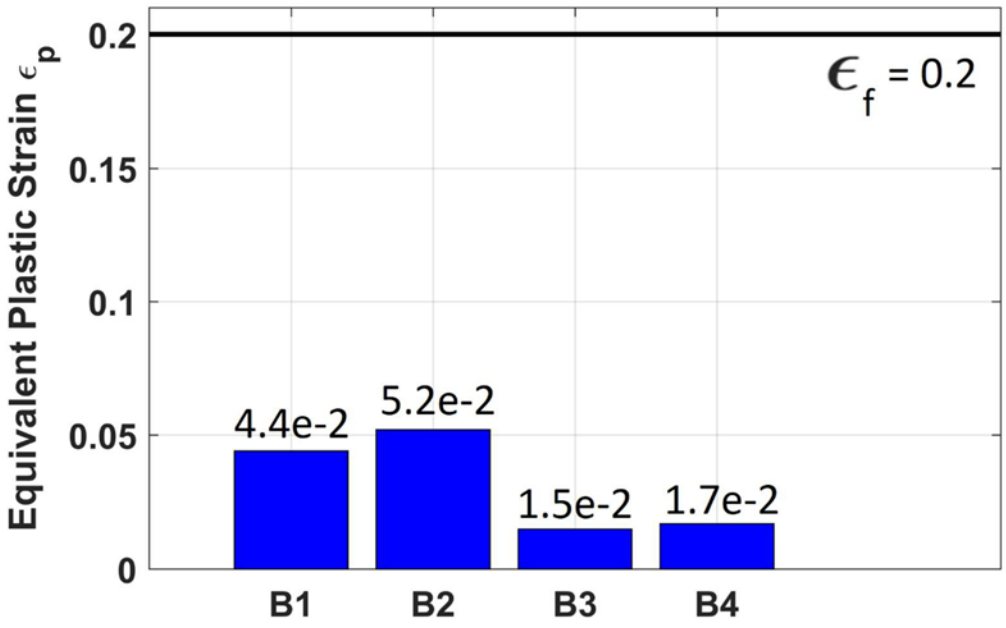

Figure 54 Equivalent plastic strain for bracing B1, B2, B3, B4 at full depth fracture

5.6 Conclusion

In this study fatigue reliability and redundancy of a two-girder steel bridge was examined. The finite element software ABAQUS was used to generate four different numerical models:

- A bridge model without crack subjected to the fatigue truck was used to determine the stresses at the location, at which in subsequent simulations the crack was initiated.
- A bridge model subjected to the fatigue truck with increasing crack length was used to compute the stress intensity factor for each crack length until full-depth fracture.
- A bridge model including residual stresses due to welding at the bottom flange and the longitudinal stiffener was used to evaluate the stress intensity factors in the compression zones.

- A bridge model subjected to the maximum design load was used to determine the equivalent plastic strain and compared to the failure strain of steel to evaluate the redundancy.

The finite element analysis was combined with Monte Carlo simulation to account for variation in the loading and the material properties. A simulation with 50 iterations was conducted to evaluate the stress at the future crack location. Furthermore, the stress intensity factor was evaluated with randomly varying load and young's modulus for each crack length that it takes for the crack to travel through the girder in 0.08m increments until fracture. The results are 50 independent stress intensity factors for each crack length.

The Paris Law is utilized to determine the number of cycles required for the crack to open one increment while treating the crack propagation parameters C and m as random variables. The critical crack length and the number of cycles to failure are estimated for material toughnesses of $50MPa(m)^{1/2}$ and $75MPa(m)^{1/2}$. For each of the previously determined stress intensity factors the simulation was conducted 10,000 times. Afterwards, different inspection intervals are used to compute the probability of failure and the corresponding reliability index. Finally, the redundancy of the bridge was assessed by comparing the equivalent plastic strain at failure to the failure strain of the steel. The outcome of this study is as follow:

1. The variation in loading and young's modulus resulted in a large scatter in the applied stresses.
2. The probability that the stresses at the bottom flange exceed the fatigue threshold of $18MPa(m)^{1/2}$ and a crack initiates at the weld connecting the bottom lateral to the girder is about 45%.

3. The tension and compression zones due to residual stresses do not significantly influence the crack propagation and therefore the effective stress intensity range ΔK_{eff} equals K_{max} from the applied load.
4. Treating the crack propagation parameters C and m as random variables in the Paris Law resulted in a very large scatter in the crack propagation rate.
5. Increasing the material toughness from 45MPa$(m)^{1/2}$ to 65MPa$(m)^{1/2}$, 75MPa$(m)^{1/2}$ and 95MPa$(m)^{1/2}$ led to a significant decrease of the probability of failure for the same inspection interval.
6. The probability index decreases with increasing number of cycles per inspection interval.
7. The maximum achievable reliability index is 4 for an inspection interval of 200,000.
8. Probabilistic analysis is necessary for determining the fatigue life of a structure due to the large scatter in the fatigue data.
9. The reliability analysis and the presented results provide a framework for decision making for specifying inspection intervals.
10. The equivalent plastic strain never exceeds the failure strain of A36 and therefore the structure has sufficient residual capacity.

REFERENCES

AASHTO. (2012). AASHTO LRFD Bridge Desigin Specification. Washington, DC. http://doi.org/978-1-56051-523-4

Abaqus/CAE User's Guide. (2014). Providence, RI: Dassault Systèmes. Retrieved from abaqus.software.polimi.it/v6.14/books/usi/default.htm

Anderson, T. L. (2005). Fracture Mechanics: Fundamentals and Applications (2nd ed.). Boca Raton, FL: Taylor & Francis Group, LLC.

Barsom, J. M. (1975). Development of the AASHTO fracture-toughness requirements for bridge steels. Engineering Fracture Mechanics, 7(3), 605–618. http://doi.org/10.1016/0013-7944(75)90060-0

Besterfield, G. H., Liu, W. K., Lawrence, M. A., & Belytschko, T. (1991). Fatigue crack growth reliability by probabilistic finite elements. Computer Methods in Applied Mechanics and Engineering, 86(3), 297–320. http://doi.org/10.1016/0045-7825(91)90225-U

Broek, D. (1989). The Practical Use of Fracture Mechanics. Dordrecht: Kluwer Academic Publishers.

Bs-7910. (1997). Guide to methods for assessing the acceptability of flaws in metallic structures. BSI Standards Publication.

Connor, R., Dexter, R., & Mahmoud, H. (2005). NCHRP Synthesis 354: Inspection and Management of Bridges with Fracture-Critical Details. Transportation Research Board, National. Retrieved from http://scholar.google.com/scholar?hl=en&btnG=Search&q=intitle:NCHRP+SYNTHESIS+354#0

Daniels, J. H., Kim, W., & Wilson, J. L. (1989). NCHRP Report 319: Recommended Guidelines for Redundancy Design and Rating of Two-Girder Steel Bridges. Washington, DC.

Daniels, J. H., Wilson, J. L., & Chen, S. S. (1987). Redundancy of simple span and two-span welded steel two-girder bridges , Final Report , September, (September), 282.

Failla, K. S. (1985). New Mianus Bridge Report Disputes Earlier Study. Civil Engineering, 55(4).

Faulkner, D. (1975). A Review of Effective Plating to be Used in the Analysis of Stiffened Plating in Bending and Compression. Journal of Ship Research, 19(1), 1–17.

Feng, G. Q., Garbatov, Y., & Guedes Soares, C. (2012). Fatigue reliability of a stiffened panel subjected to correlated crack growth. Structural Safety, 36–37, 39–46. http://doi.org/10.1016/j.strusafe.2011.09.002

Fisher, J. W., Kulak, G. L., & Smith, I. F. C. (1998). National Steel Bridge Alliance A Fatigue Primer for Structural Engineers A Note of Caution.

Frangopol, D. M., & Curley, J. P. (1987). Effects of Damage and Redundancy on Structural Reliability. Journal of Structural engineering/ASCE, 113(7), 1533–1549. http://doi.org/10.1061/(ASCE)0733-9445(1987)113:7(1533)

Furuta, H., Shinozukam, M., & Yao, J. T. P. (1985). Probabilistic and Fuzzy Representation of Redundancy in Structural Systems. Palma de Malorca, Spain: First International Fuzzy Systems Associated Congress.

Galambos, T. V., & Ravindra, M. K. (1978). Properties of Steel for Use in LRFD. Journal of the Structural Division, 104(9), 1459–1468.

Hartley, D., & Ressler, S. (1989). After-Fracture Redundancy of Steel Bridges: A Review of Published Research. Bethlehem, Pa.

Inglis, C. E. (1913). Stresses in a Plate Due to the Presence of Cracks and Sharp Corners. Transaction of the Institute of Naval Architects, 55, 219–241.

Irwin, G. R. (1957). Analysis of Stresses and Strains Near the End of a Crack Traversing a Plate. Journal of Applied Mechanics, 24(September), 361–364. http://doi.org/no DOI

Lwin, M. M. (2012). Memorandum: Clarification of Requirements for Fracture Critical Members.

Mahmoud, H. N., & Dexter, R. J. (2005). Propagation rate of large cracks in stiffened panels under tension loading. Marine Structures, 18(3), 265–288. http://doi.org/10.1016/j.marstruc.2005.09.001

Mahmoud, H., & Riveros, G. (2014). Fatigue reliability of a single stiffened ship hull panel. Engineering Structures, 66, 89–99. http://doi.org/10.1016/j.engstruct.2014.02.007

Melchers, R. E. (1999). Structural Reliability Analysis and Prediction (Second Edi). Chichester: John Wiley & Sons Ltd.

Norita, T. (1985). Fiber reinforced composite materials. Kobunshi, 34(11), 910–913. http://doi.org/10.1295/kobunshi.34.910

Nowak, A. S. (1995). CALIBRATION OF LRFD BRIDGE CODE. Journal of Structural Engineering, 121(8), 1245–1251.

Paris, P. C., & Erdogan, F. (1963). A Critical Analysis of Crack Propagation Laws. Journal of Basic Engineering. http://doi.org/10.1115/1.3656900

phimeca. (2016). phimeca. Retrieved December 10, 2016, from http://www.phimeca.com/PhimecaSoft-107?lang=en

Ripling, E. J., & Crosley, P. B. (1982). Crack Arrest Fracture Toughness of Structural Steel (A36). Welding Research, 65–74.

Robert, R., Irwin, G. R., Krishna, G. V., & Yen, B. T. (1974). Fracture Toughness of Bridge Steel - Phase II. Report FHWA-RD-74-59. Washington, DC.

Rolfe, S. T., & Barsom, J. M. (1999). Fracture and Fatigue Control in Structures: Application of Fracture Mechanics (3rd ed.). West Conshohocken, Pa: American Society for Testing and Materials.

Wöhler, A. (1870). Über die Festigkeitsversuche mit Eisen und Stahl. Zeitschrift Für Bauwesen, 20.